DOT/FAA/AR-04/45,P2

Office of Aviation Research
Washington, D.C. 20591

Lightweight Ballistic Protection of Flight-Critical Components on Commercial Aircraft

Part 2: Large-Scale Ballistic Impact Tests and Computational Simulations

December 2004

Final Report

This document is available to the U.S. public through the National Technical Information Service (NTIS), Springfield, Virginia 22161.

U.S. Department of Transportation
Federal Aviation Administration

NOTICE

This document is disseminated under the sponsorship of the U.S. Department of Transportation in the interest of information exchange. The United States Government assumes no liability for the contents or use thereof. The United States Government does not endorse products or manufacturers. Trade or manufacturer's names appear herein solely because they are considered essential to the objective of this report. This document does not constitute FAA certification policy. Consult your local FAA aircraft certification office as to its use.

This report is available at the Federal Aviation Administration William J. Hughes Technical Center's Full-Text Technical Reports page: actlibrary.tc.faa.gov in Adobe Acrobat portable document format (PDF).

Technical Report Documentation Page

1. Report No.	2. Government Accession No.	3. Recipient's Catalog No.
DOT/FAA/AR-04/45,P2		

4. Title and Subtitle	5. Report Date
LIGHTWEIGHT BALLISTIC PROTECTION OF FLIGHT-CRITICAL COMPONENTS ON COMMERCIAL AIRCRAFT PART 2: LARGE-SCALE BALLISTIC IMPACT TESTS AND COMPUTATIONAL SIMULATIONS	December 2004
	6. Performing Organization Code P11722 and P12100
7. Author(s) Donald A. Shockey, David C. Erlich, and Jeffrey W. Simons	8. Performing Organization Report No.
9. Performing Organization Name and Address SRI International 333 Ravenswood Avenue Menlo Park, CA 94025	10. Work Unit No. (TRAIS)
	11. Contract or Grant No. 01-C-AW-UCB SUBAGREEMENT SA3447
12. Sponsoring Agency Name and Address U.S. Department of Transportation Federal Aviation Administration Office of Aviation Research Washington, DC 20591	13. Type of Report and Period Covered Final Technical Report 12/2001–12/2002
	14. Sponsoring Agency Code ANE-100, ANM-100

15. Supplementary Notes

The Federal Aviation Administration William J. Hughes Technical Center COTR was Donald Altobelli.

16. Abstract

SRI International collaborated with the University of California at Berkeley and The Boeing Company to investigate lightweight ballistic protection of commercial aircraft from engine fragments. SRI's role was to perform large-scale impact tests of barriers made from multilayer high-strength fabric and to computationally simulate the tests with a finite element model. This document (which is part 2 of the report) describes the tests and the model and presents the findings and remaining issues. Part 1 of the report includes small-scale ballistic impact tests and computational simulation by the University of California at Berkeley. Part 3 contains Zylon® yarn material tests conducted by The Boeing Company.

17. Key Words	18. Distribution Statement
Aircraft engine fragments, Fragment barriers, Uncontainment, Zylon	This document is available to the public through the National Technical Information Service (NTIS) Springfield, Virginia 22161.

19. Security Classif. (of this report)	20. Security Classif. (of this page)	21. No. of Pages	22. Price
Unclassified	Unclassified	72	

Form DOT F 1700.7 (8-72) Reproduction of completed page authorized

TABLE OF CONTENTS

		Page
EXECUTIVE SUMMARY		ix
1.	INTRODUCTION AND BACKGROUND	1-1
2.	LARGE-SCALE BALLISTIC IMPACT TESTS	2-1
2.1	Test Design and Procedures	2-1
2.1.1	Impactors	2-2
2.1.2	Target Configurations	2-3
2.1.3	Fabric Materials	2-6
2.1.4	Test Procedures	2-7
2.2	Test Results	2-8
2.2.1	Test Repeatability	2-13
2.2.2	Comparison of Fabric Materials	2-14
2.2.3	Zy35 Results for Configuration A	2-16
2.2.4	Zy35 Results for Configuration B	2-18
2.2.5	Fabric Tear-Off From Pegs	2-21
2.2.6	Comparison of Zy35 Results for Configurations A and B	2-22
2.2.7	Fabric Barrier Damage	2-23
2.3	Summary of the Ballistic Tests	2-25
2.3.1	Key Findings	2-26
2.3.2	Questions and Issues	2-27
2.3.3	Suggested Future Work	2-28
3.	METHODS FOR CUTTING HOLES IN ZYLON FABRIC	3-1
3.1	Previous Methods	3-1
3.2	Current Methods	3-1
3.3	Recommended Future Method—Laser Cutting	3-1
4.	FINITE ELEMENT ANALYSIS	4-1
4.1	Finite Element Model	4-1
4.2	Finite Element Mesh	4-2
4.3	Material Models	4-3
4.4	Slideline Treatment	4-4
4.5	Model Results	4-4
4.6	Fabric Deformation and Failure	4-8

4.6.1 Test 1 4-8
4.6.2 Test 3 4-9
4.6.3 Test 17 4-10

4.7 Fabric Failure Mechanism 4-10

5. SUMMARY AND RECOMMENDATIONS 5-1

5.1 Summary 5-1
5.2 Recommendations 5-2

6. REFERENCES 6-1

APPENDIX A—PLAN FOR BALLISTIC TESTING OF ZYLON FABRIC

LIST OF FIGURES

Figure Page

2-1 Six-in.-Bore Gas Gun at SRI's Remote Test Site 2-1

2-2 Alloy Steel Impactors and Sabot 2-2

2-3 Rigid Ladder Frame Test Setup (Configuration A), as Viewed From Behind the Target 2-3

2-4 Rigid Ladder Frame Test Setup (Configuration A), Without the Aluminum Backing Sheet 2-4

2-5 The 97-cm- (38-in.)-Square Frame Test Setup (Configuration B), as Viewed From Behind the Target 2-5

2-6 The 97-cm- (38-in.)-Square Frame Test Setup (Configuration B), Without the Aluminum Backing Sheet 2-5

2-7 View of the Test Setup From the Camera Location 2-7

2-8 High-Speed Digital Video Camera and Ring Lights 2-8

2-9 Selected Video Camera Frames From Test 3 2-11

2-10 Selected Video Camera Frames From Test 13 2-12

2-11 Selected Video Camera Frames From Test 15 2-13

2-12	Residual Velocity Versus Impact Velocity Data for Repeat Tests With Full Penetration	2-14
2-13	Energy Absorption Results for Various Fabric Materials	2-15
2-14	Energy Absorption Results for Zy35 Configuration A Tests	2-16
2-15	Energy Absorption Results for Zy35 Configuration A Tests With the Small Impactor	2-16
2-16	Views of Damage to Aluminum Backing Sheet From Configuration A Test	2-17
2-17	Energy Absorption Results for Zy35 Configuration B Tests	2-18
2-18	Views of Target After Configuration B Test 39 (With No Penetration)	2-19
2-19	Views of Aluminum Backing Sheet After Configuration B Test 39	2-20
2-20	Views of Aluminum Backing Sheet After Configuration B Test 42 (Complete Penetration)	2-20
2-21	Posttest Views of Aluminum Backing Sheets From Small Impactor Configuration B Tests	2-21
2-22	Fabric After Tear Off From Pegs in Two Configuration B Tests Without Aliminum Backing Sheet	2-22
2-23	Comparison of Energy Absorption Results for Configurations A and B Without Aluminum Backing Sheet	2-22
2-24	Typical Damage to Zy35 Fabric in Impact and Pegged Areas for Higher SEA Tests	2-25
3-1	Three Views of a 2.54-cm- (1-in.)-Diameter Hole Laser-Cut Into 48 Plies of Zy35 Fabric	3-2
4-1	Finite Element Model of Frame Configurations	4-1
4-2	Impactor Model	4-2
4-3	Simulations of Configuration A Tests With the Small Impactor	4-5
4-4	Simulation of Configuration A, Large Impactor	4-6
4-5	Simulation of Configuration B Tests	4-6
4-6	Simulations of Configuration A vs B	4-7
4-7	Simulation of Off-Center Tests	4-7

4-8 Simulations of Roll Angle 4-8

4-9 Fabric Deformation for Test 01 4-9

4-10 Fabric Deformation for Test 03 4-9

4-11 Fabric Deformation for Test 10 4-10

4-12 Fabric Tearing at the Impactor 4-11

4-13 Fabric Tearing at the Attachment 4-11

LIST OF TABLES

Table Page

2-1 Fabric Materials Tested 2-6
2-2 Parameters and Energy Absorption Results for the Ballistic Impact Tests 2-9
2-3 Fabric Damage in Ballistic Impact Tests 2-23
4-1 Constants for Zylon 4-3
4-2 Results of Model Simulations for CHES Tests 4-4
4-3 Ratio of Model to Experiment Energy Absorbed 4-5

LIST OF ACRONYMS

cm	Centimeter
CO_2	Carbon dioxide
f/s	Frames per second
FAA	Federal Aviation Administration
g	Grams
g/cm^2	Gram per square centimeter
kft-lb	Kilo foot-pound
kJ	Kilojoules
ksi	Thousand pounds per square inch
lb/ft^2	Pound per square foot
m/s	Meter per second
MPa	Milipascals
NASA	National Aeronautics and Space Administration
PBO	Poly-benzoxazole (generic)
SEA	Specific energy absorbed
UC	University of California

EXECUTIVE SUMMARY

Uncontained turbine engine failures remain a major cause of commercial aircraft incidents and has led to catastrophic aircraft accidents. To mitigate the effect of uncontained engine debris on critical aircraft components, the Federal Aviation Administration (FAA), under the Aircraft Catastrophic Failure Prevention Program, has sponsored research to develop lightweight barrier systems for aircraft and to develop the computational capability to design these barriers.

The goal of this research project, carried out under the auspices of the FAA Airworthiness Assurance Center of Excellence, was to use the technical strengths and experience of The Boeing Company, SRI International, and the University of California, Berkeley, to develop rotor burst fragment shielding and finite element modeling methodology. Since the development of an experimental set of data to support the calibration of the finite element models was essential, various experimental methods were used to measure material and structural response of the fabrics.

Each member of the team developed a report describing the details and the findings of their research task. The comprehensive report "Lightweight Ballistic Protection of Flight Critical Components on Commercial Aircraft," is comprised of the following three parts.

- Part 1: "Small-Scale Testing and Computational Analysis" by the University of California, Berkeley.
- Part 2: "Large-Scale Ballistic Impact Tests and Computational Simulations" by SRI International.
- Part 3: "Zylon Yarn Tests" by The Boeing Company.

To evaluate the efficacy and practicality of Zylon® fabric for fragment barriers on commercial transport aircraft, SRI performed large-scale ballistic tests on fabric barrier structures. SRI also simulated the experiments with a finite element model of the barrier to develop further and demonstrate a capability to compute the response of a barrier structure to given fragment threats. This report presents the procedures and results of the SRI effort.

Barrier structures consisting of multiple layers of Zylon and other fabrics in specific frame configurations were tested against simulated turbine fragments of specified mass and velocity in The 6-in.-Bore Gas Gun Facility at SRI's remote experiment site. The tests examined two frame conditions, large and small impactors, center and off-center impact locations, and a range of roll angles. The velocities and orientation of the projectile as it approached and as it exited the barrier were measured with a high-speed camera. The stopping power of the barriers was determined from the incoming and exiting velocities as the energy absorbed per unit areal density of the barrier. The damage mechanisms were determined by examining the tearing at the impact site and the sites of attachment to the frame.

The experiments and computations reported here suggest that lightweight barriers of ballistic fabric are practical solutions to uncontained engine debris protection.

1. INTRODUCTION AND BACKGROUND.

To mitigate the effect upon critical aircraft components of uncontained fragments from turbine engine failures, the Federal Aviation Administration (FAA), under the Aircraft Catastrophic Failure Prevention Program, has sponsored research to develop lightweight barrier systems for aircraft and to develop a physics-based computational capability for designing these barriers.

Laboratory gas gun tests in which small-scale fragment simulators impacted a variety of potential barrier materials showed that woven fabrics of high-strength polymers such as aramids (e.g., Kevlar®), polyethylenes (e.g., Spectra), and particularly a poly-benzoxazole (PBO) (e.g., Zylon®) had very high energy absorption per unit weight in impact tests against fragment simulators. Full-scale fragment impact tests against aircraft fuselage sections fortified with the woven fabric confirmed the suitability of these materials as fragment barriers.

SRI International developed a computational capability for high-strength fabrics by modeling the geometry, properties, and interactions of individual yarns within the woven fabric. Input to the model was provided by laboratory tests to measure yarn tensile and friction properties; quasi-static penetration tests to measure the evolution and phenomenology of fabric deformation and failure; and projectile impact tests to measure the effects of fabric material, mesh density, boundary conditions (how a fabric is gripped), and projectile sharpness. The model was implemented in the LS-DYNA3D finite element code and used to simulate the failure behavior of yarns and fabrics under various scenarios. The resulting insights assisted barrier design. A simplified version of the detailed computational model has been developed to assist the transport aircraft industry in designing engine fragment barriers.

At the Fourth FAA Uncontained Engine Debris Characterization Modeling and Mitigation Workshop, The Boeing Company expressed interest in the potential of Zylon for protecting specific flight-critical components such as the rotary auxiliary turbine system and auxiliary fuel tanks for long-distance flights. With encouragement from the FAA, SRI and Boeing discussed initiating a program in this area and invited University of California (UC) Berkeley, with its expertise in both ballistic impacts and finite element analyses, to join in these discussions.

UC Berkeley, together with SRI and Boeing, were granted an FAA Airworthiness Assurance Center of Excellence grant to do an experimental and computational study to transition the results of the research to an industrial application, namely, using Zylon ballistic fabric barriers for protection against transport airplane rotor burst fragments. Ballistic tests were performed to characterize the ballistic effectiveness of high-strength fabric barriers against a range of realistic fragment threats in specific test cases of interest to transport aircraft. SRI's finite element Zylon computational model was then adapted, as needed, to address these specific shielding scenarios, verified by comparison with the ballistic test results, and transferred to Boeing. Various mechanical, thermal, environmental, and compatibility tests were performed to address the suitability of the high-strength fabric material for use on transport aircraft. This report summarizes the results of this study.

SRI's effort in the UC Berkeley and Boeing program is presented in this part (part 2) of the comprehensive report. The objective of this program was to evaluate the efficacy and practicality of high-strength fabric for fragment barriers on commercial transport aircraft. SRI's part was to (1) perform large-scale ballistic tests to investigate how off-center impact, fragment orientation, and environmental exposure affect ballistic performance and (2) use the fabric design model to simulate the experiments to demonstrate the capability to compute the response of a barrier structure to given fragment threats. The procedures and results of this effort are presented in the following sections.

2. LARGE-SCALE BALLISTIC IMPACT TESTS.

The goal for the large-scale impact tests was to evaluate the ability of high-strength fabrics to protect aircraft from engine fragments, to evaluate SRI's computational fabric barrier model, and to develop a reliable ballistic database for these fabrics. The specific tests were based on various impactor and target scenarios selected by Boeing. Appendix A contains the original test plan written by Boeing. This plan was modified due to lack of funding to do all the tests and the report summarizes the test results.

Impactor masses and velocities were chosen to be typical of those in actual turbine engine fragment scenarios. The target configurations, although having some features similar to fuselage walls, were selected primarily to provide well-defined fabric boundary conditions conducive to computational modeling, rather than to simulate an actual fuselage. Zylon® AS 35x35 fabric was selected as the baseline test material; three other materials were also included in the study for comparison.

2.1 TEST DESIGN AND PROCEDURES.

The impact tests were performed during the period from June to October 2002, using The 6-in.-Bore Gas Gun located at the Corral Hollow Experimental Station, SRI's remote test site in Livermore, CA (see figure 2-1).

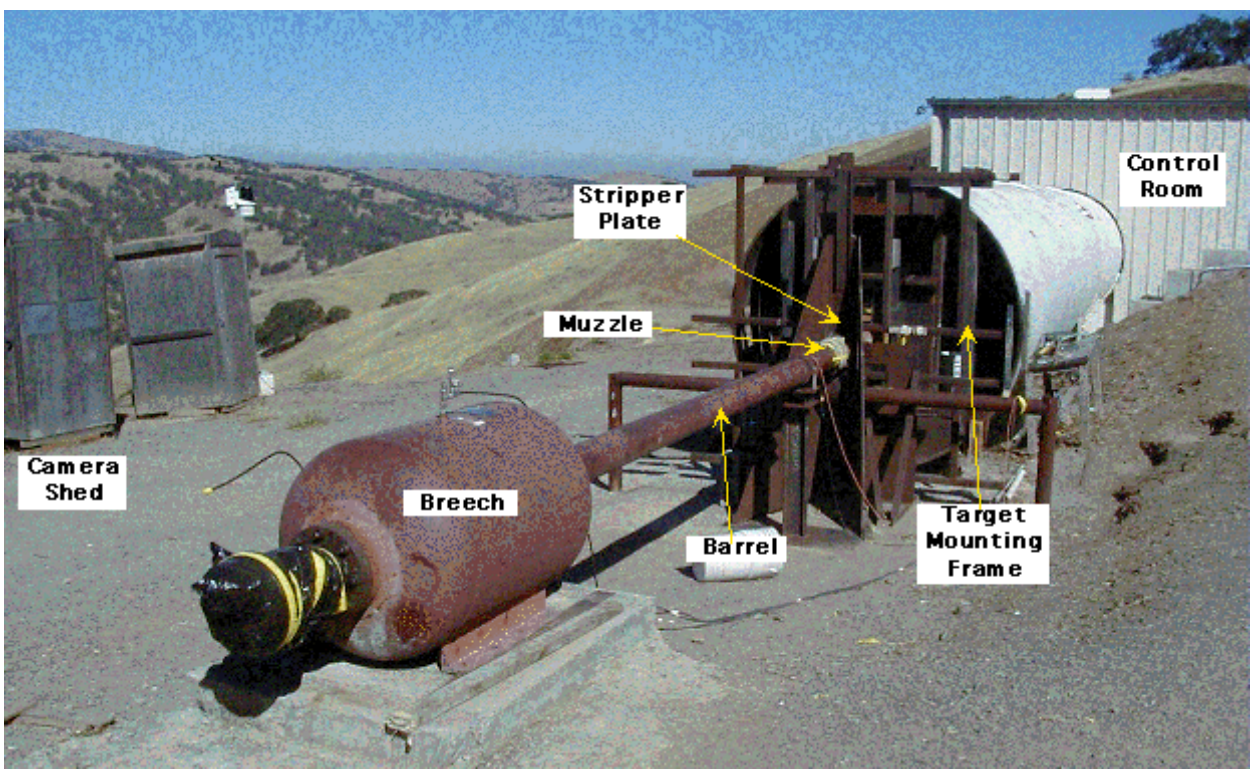

FIGURE 2-1. SIX-in.-BORE GAS GUN AT SRI'S REMOTE TEST SITE

2.1.1 Impactors.

The two different alloy steel impactors used in these tests are shown in figures 2-2(a) and 2-2(b). The small impactor weighed 126-128 g (0.28 lb) and had dimensions of 5.08 by 5.08 by 0.63 cm (2 by 2 by 0.25 in.), while the large impactor weighed 989-992 g (2.2 lb) and had dimensions of 10.16 by 10.16 by 1.27 cm (4 by 4 by 0.5 in.). The front and side edges of the impactors were rounded to a radius of curvature of approximately 0.04 cm (0.015 in.).

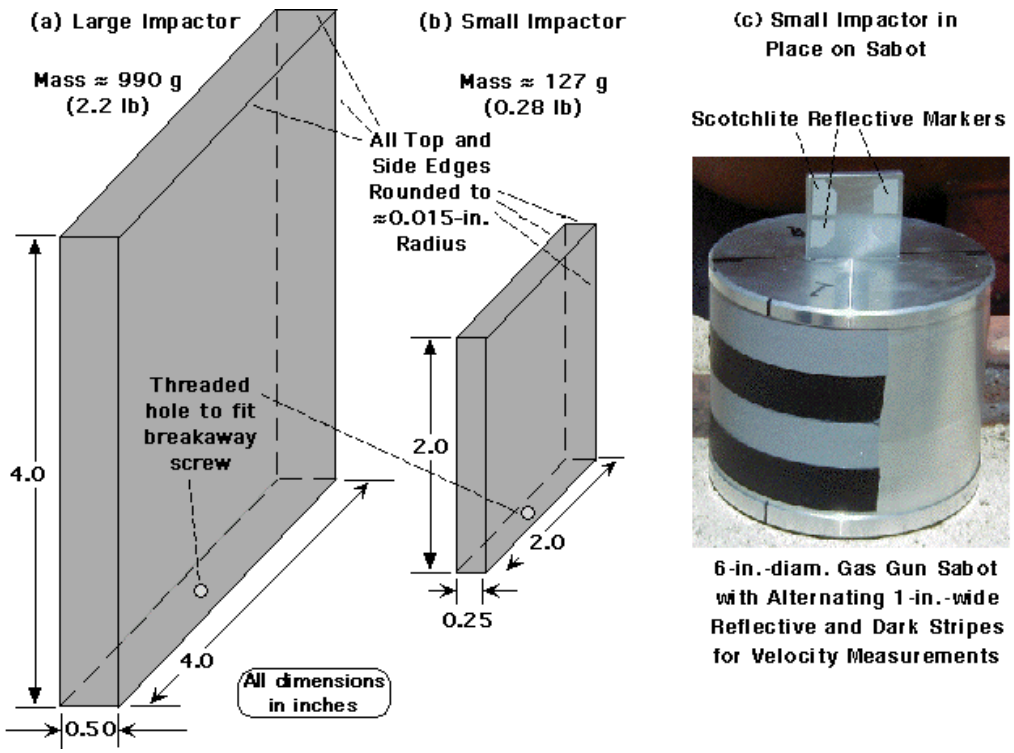

FIGURE 2-2. ALLOY STEEL IMPACTORS AND SABOT

The impactors, marked with Scotchlite* highly reflective tape fiducials, were positioned in a slot at the front of 15-cm- (6-in.)-diameter aluminum sabots (see figure 2-2(c)). The sabots also had reflective markers taped around a portion of their peripheries. These 2.54-cm- (1-in.)-wide markers, alternating with 2.54-cm- (1-in.)-wide strips of dark tape, were used in conjunction with optical fiber light sensors located near the muzzle end of the gun barrel as a backup impact velocity recording method.

Impact velocities ranged from 142 to 277 m/s (466 to 909 f/s), and the impact kinetic energies ranged from 1.3 to 26 kJ (0.95 to 19.2 kft-lb). The intended impact roll angle was 45° for most tests—this was the roll angle for which a slight variation would least change the number of total yarns directly impacted. A few tests had intended impact rolls of 0° (longest impact edge vertical) or 90° (longest impact edge horizontal). The intended impact pitch and yaw were 0° for all tests.

* Obtained from Virtual Backgrounds, San Marcos, TX.

2.1.2 Target Configurations.

Two target configurations were used in the tests. In both configurations, the fabric barriers were supported by rigid steel frames made of strong hollow rectangular box beams, designed to prevent plastic deformation in the frames during the tests. The box beams had dimensions of 7.6 by 5.1 cm (3.0 by 2.0 in.), a wall thickness of 0.63 cm (0.25 in.), and rounded edges with a radius of curvature of approximately 1.3 cm (0.5 in.). The box beams were made from A500C carbon steel, which has, according to manufacturer's specifications, a minimum tensile strength of 345 MPa (50 ksi), a minimum yield strength of 428 MPa (62 ksi), and a minimum elongation to failure of 21%.

The fabric was positioned on the front of the box beam frame and pegged in place by bolts that fit through ≈ 1.3-cm- (≈ 0.5-in.)-diameter holes that were cut into the fabric. The bolts were 1/2-in. -20, made from grade 8 steel alloy (130-ksi yield strength, 150-ksi ultimate tensile strength), chosen to be strong enough to avoid plastic deformation during the tests.

The first configuration, shown in figure 2-3, was the rigid ladder frame (Configuration A), which consists of four horizontal beams, centered 32.3 cm (12.7 in.) apart, and welded between two vertical beams, centered 61 cm (24 in.) apart. The fabric, which is approximately 124 cm tall by 89 cm wide (49 in. tall by 35 in. wide), was pegged to the beam with eight bolts, located on the two vertical beams at their junction with the horizontal beams. The vertical beams were bolted above and below the fabric region to the gas gun facility's target-mounting frame. The setup for configuration A is shown in figure 2-4.

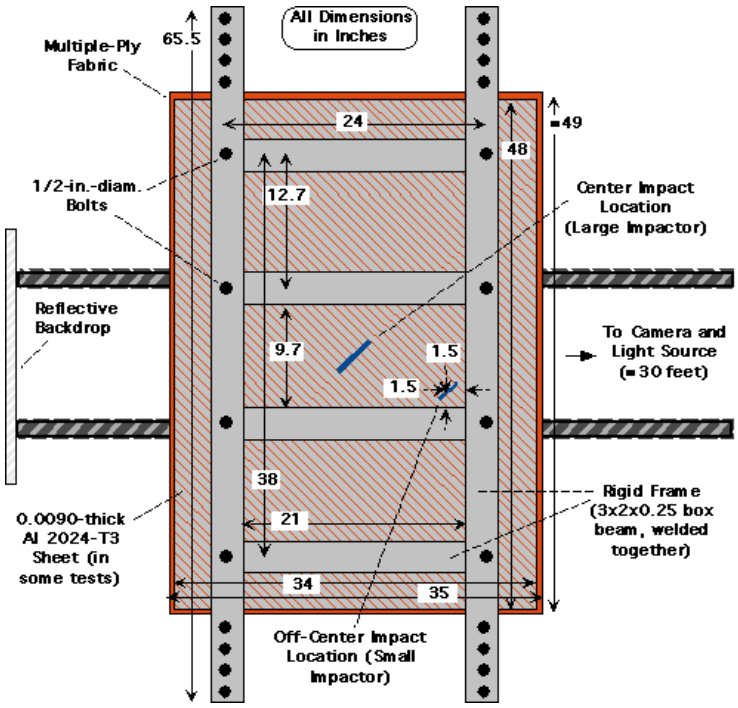

FIGURE 2-3. RIGID LADDER FRAME TEST SETUP (CONFIGURATION A), AS VIEWED FROM BEHIND THE TARGET

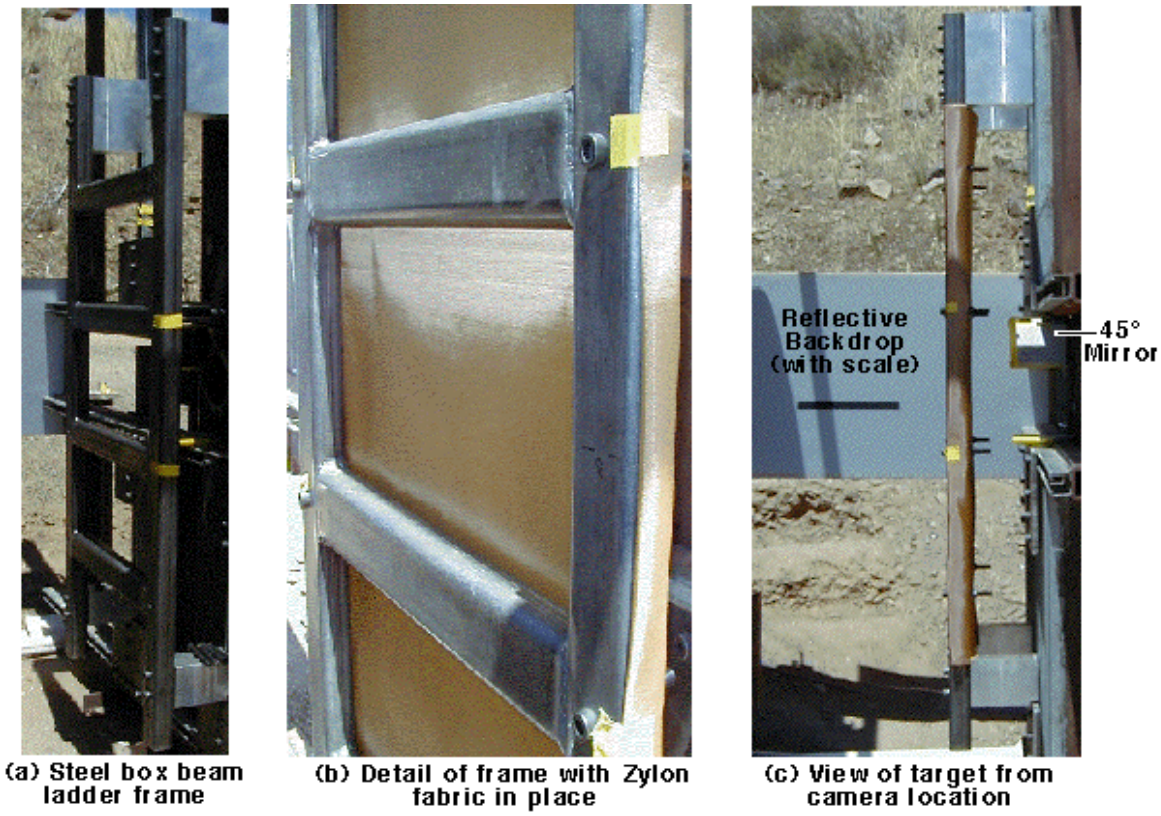

FIGURE 2-4. RIGID LADDER FRAME TEST SETUP (CONFIGURATION A), WITHOUT THE ALUMINUM BACKING SHEET

For most tests, the impact location was at the target center, midway between the two inner horizontal beams. A few tests (all involving the small impactors), had an off-center impact location (as shown in figure 2-3), with the impact center 3.8 cm (1.5 in.) away from both the vertical and horizontal beam (or 8.1 cm (3.2 in.) from the center of the nearest peg). For some tests, a 0.229-cm- (0.090-in.)-thick aluminum 2024-T3 alloy backing sheet was positioned between the fabric and the frame.

The second configuration, shown in figure 2-5, was the 97-cm- (38-in.)-square frame (Configuration B), which consisted of two vertical beams only (the horizontal beams needed to keep the frame rigid are above and below the fabric and do not affect the fabric deformation), centered 97 cm (38 in.) apart, to which the approximately 124-cm- (49-in.)-square fabric was pegged every 32.3 cm (12.7 in). For most tests, the impact location was at the target center, midway between the two vertical beams. A few tests (involving both the large and small impactors), had off-center impact locations, with the impact center as close as feasible to one beam 16.5 or 23.4 cm (6.5 or 9.2 in.) from the center of the nearest peg). The setup for configuration B is shown in figure 2-6.

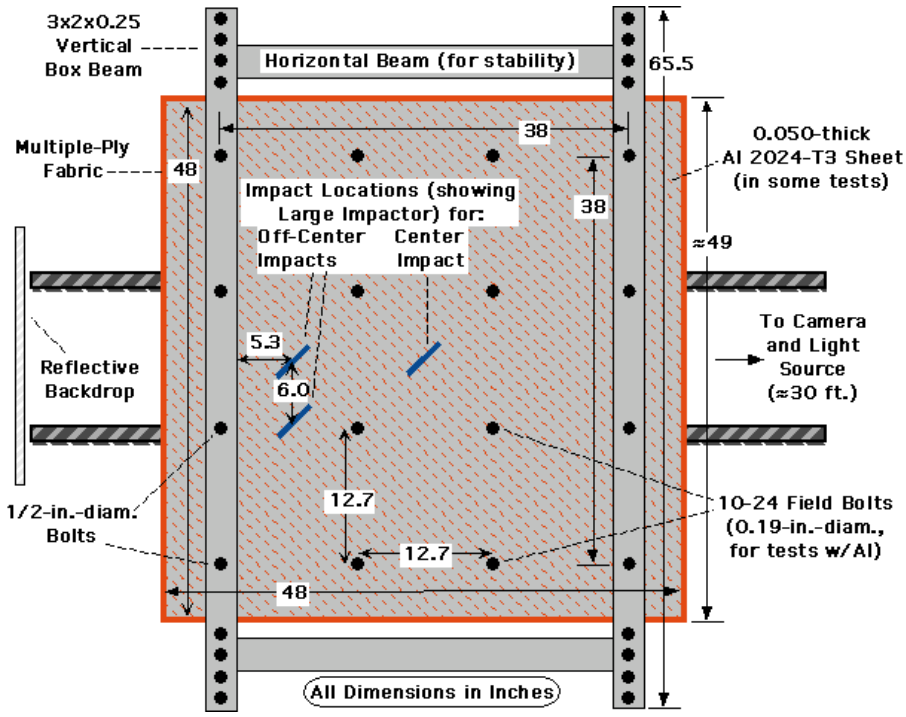

FIGURE 2-5. THE 97-cm- (38-in.)-SQUARE FRAME TEST SETUP (CONFIGURATION B), AS VIEWED FROM BEHIND THE TARGET

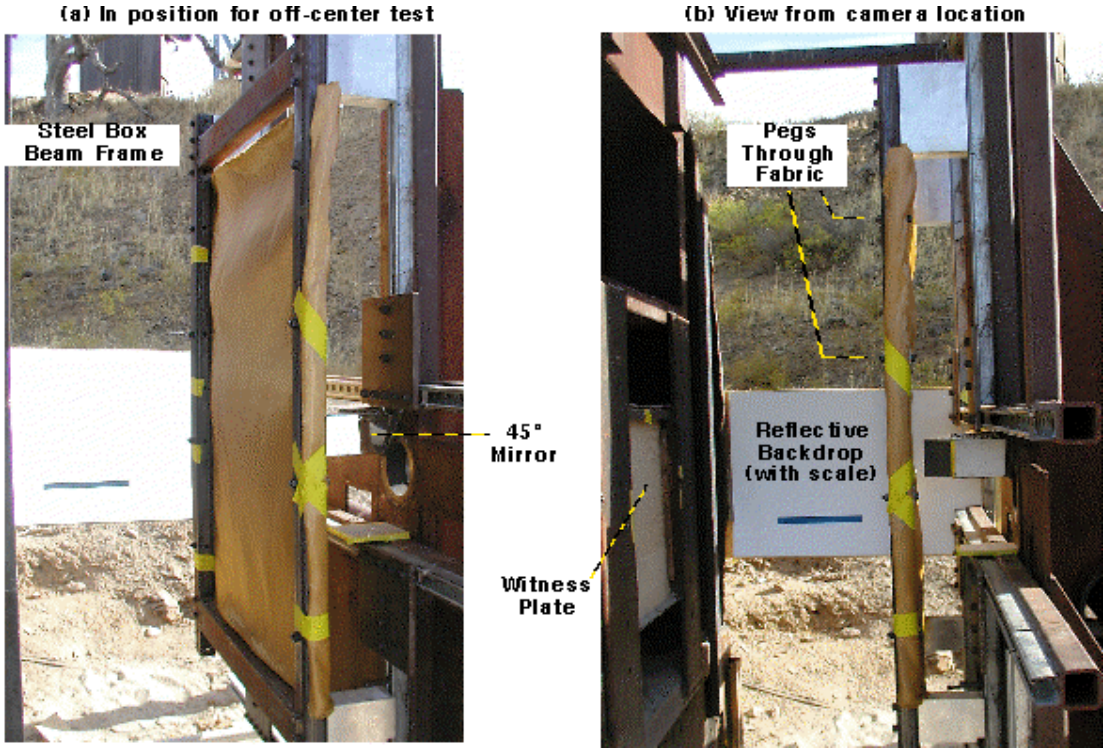

FIGURE 2-6. THE 97-cm- (38-in.)-SQUARE FRAME TEST SETUP (CONFIGURATION B), WITHOUT THE ALUMINUM BACKING SHEET

For some tests, a 0.127-cm- (0.050-in.)-thick aluminum 2024-T3 backing sheet was positioned between the fabric and the frame. For these tests, eight field bolts (no. 10-24 bolts, ≈ 0.48 cm (≈ 3/16 in.) in diameter, with nuts and fender washers) in a 32.2-cm- (12.7-in.)-square lattice pattern, as shown in figure 2-5, were used to keep the fabric positioned next to the backing sheet.

2.1.3 Fabric Materials.

Four fabric materials were used in these tests, all woven in a simple weave style by Lincoln Fabrics LTD. of Ontario, Canada. The baseline material was a Zylon AS 35x35 weave (designated light Zylon or Zy35) with 500-Denier yarns. The other materials were

- a Zylon AS 17x17 weave (designated heavy Zylon, or Zy17), with ≈1500-Denier yarns,
- a Kevlar® KM-2 29x29 weave (designated Kev29), with ≈600-Denier yarns, designed to closely match the areal density of the baseline Zylon, and
- environmentally exposed (EE) Zylon baseline material (Zy35 fabric subjected to 160°F and 85% humidity for 3 weeks at Boeing) designated E.E. Zy.

The relevant properties of these materials are given in table 2-1.

TABLE 2-1. FABRIC MATERIALS TESTED

Program Designation		Baseline Zylon (AS) (or Zy35)	Heavy Zylon (AS) (or Zy17)	Kevlar (KM-2) (or Kev29)
Trade Name		Zylon AS		Kevlar KM-2
Material		PBO		Aramid
Volume density (from manufacturer)	(g/cm^3)	1.54	1.54	1.44
Yarn Denier - as ordered	(g/9 km)	500	1500	600
Yarn Denier - measured	(g/9 km)	500	1488	595
Yarn linear density - measured	(mg/cm)	0.556	1.654	0.661
Yarn cross-sectional area†	($cm^2 \times 10^{-4}$) ($in.^2 \times 10^{-5}$)	3.61 5.59	10.74 16.64	4.59 7.11
Yarn count	(yarns/in.)	35x35	17x17	29x29
Fabric ply thickness (approx.)	(in.) (mm)	0.008 0.21	0.011 0.28	0.008 0.20
Fabric areal density - measured	(g/cm^2) (lb/ft^2) (oz/yd^2)	0.01575 0.0323 4.65	0.0223 0.0457 6.58	0.01546 0.0317 4.56
Degree of Crimp*: warp yarn fill yarns	(%)	3.1 0.6	2.2 0.9	1.2 1.2

†Calculated by dividing measured linear density by volume density.

* Elongation when straightened after removal from fabric.

Two different target thicknesses or areal densities were tested. The thinner target consisted of four plies of the baseline Zylon and had an areal density of 0.063 g/cm^2 (0.13 lb/ft^2). The thicker target consisted of twelve plies of the baseline Zylon, Kevlar, or E.E. Zylon, or eight plies of the heavy Zylon, all of which had an areal density of 0.178 to 0.189 g/cm^2 (0.365 to 0.387 lb/ft^2).

2.1.4 Test Procedures.

Figure 2-7 shows a drawing of the test setup, as viewed from the camera location. The sabot, with the impactor positioned at its front, was accelerated down the 15.2-cm- (6-in.)-bore gun barrel. Shortly after exiting the muzzle, the sabot was stopped by the stripper fixture, which consisted of soft polyethylene or dead-soft aluminum squish ring (to prevent breakup of the sabot), a Mylar® diaphragm (to prevent an air shock from deforming the fabric prior to impact), and a rigid steel stripper ring, all attached to a strong steel stripper plate.

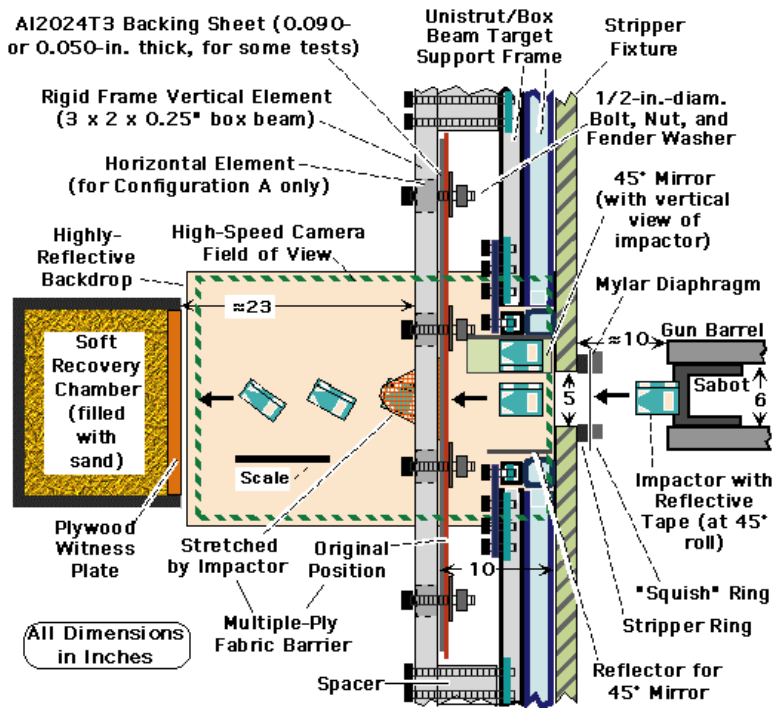

FIGURE 2-7. VIEW OF THE TEST SETUP FROM THE CAMERA LOCATION

The impactor, held to the sabot by a thin, weakened bolt, broke free of the sabot and traveled through the hole in the stripper towards the target, which was attached to a Unistrut/Box Beam support frame at a distance of about 25.4 cm (10 in.) from the back of the stripper plate. If the impactor penetrated the target, it was captured within a sand-filled, soft-recovery chamber with a plywood witness plate front cover.

The motion of the impactor and the deformation of the target were recorded during the test with a Photo-Sonics, Inc., Phantom 5 high-speed digital video camera. The camera recorded a 256- by 256- or 128- by 256-pixel region at framing rates between 7,400 and 19,800 frames per second (f/s) (mostly between 11,200 and 12,048 frames per second), with an exposure duration

of 10 μs. The field of view extended from just behind the stripper plate to nearly the front of the recovery chamber. The camera and light source were located approximately 30 feet away from the axis of the gas gun (in the directions shown in figures 2-3 and 2-5). A ring light source was used around the camera lens (see figure 2-8), which kept the light source and camera within the 1° angle of maximum reflectivity for the highly reflective Scotchlite material.

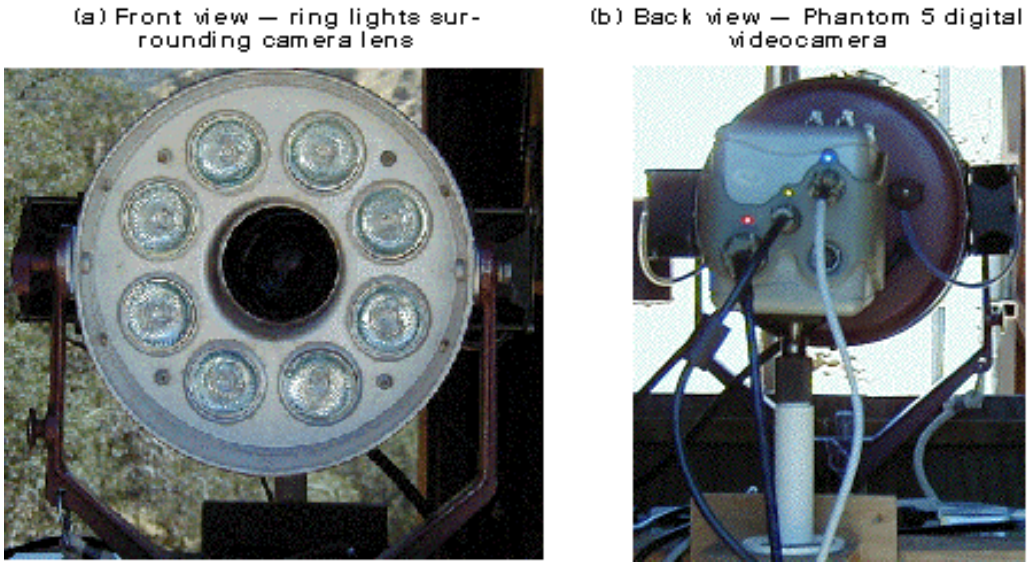

FIGURE 2-8. HIGH-SPEED DIGITAL VIDEO CAMERA AND RING LIGHTS

Two different camera and lighting methods were used. Reflections from the Scotchlite backdrop created silhouette images of the impactor and the edge of the deforming fabric (or aluminum). Scotchlite markers placed on the surfaces of the impactor produced reflected images, which were used to determine the initial impactor orientation and detect the impactor's corners when they perforated the fabric.

In addition to the direct horizontal view of the impactor, a transverse, vertical view of the impactor was obtained before impact through a 45° mirror positioned above the gun axis, extending from back of the stripper plate to roughly 2 in. away from the impact plane (4 in. for the first 22 tests). A comparison of the horizontal and vertical images allowed an accurate determination of the impactor's roll, as well as yielding both preimpact pitch and yaw data.

2.2 TEST RESULTS.

A total of 63 ballistic fabric impact tests were performed in this program. Of these, 54 tests were deemed successful, yielding complete and credible energy absorption data. (The other tests were excluded either because one or both of the relevant velocity measurements were not obtained or because the fabric barrier was subjected to premature loading from an air blast or impact by various debris.) A matrix of the parameters and some results for the 54 tests, including velocities, impact orientations, and energy absorption values, is given in table 2-2.

TABLE 2-2. PARAMETERS AND ENERGY ABSORPTION RESULTS FOR THE BALLISTIC IMPACT TESTS

Test No.[a]	Configur-ation[b]	Target		Im-pac-tor[d]	Impact				Impact Velocity		KE/AD[f] (kJ/g/cm^2)	Pen.? If not, max. defl. [g]	Residual Velocity		SEA[h] (kJ/g/cm^2)	Comments
		No. Plies	Material[c]		Loca-tion	Orientation[e] (°) Roll	Pitch	Yaw	(f/s)	(m/s)			(f/s)	(m/s)		
1	A/no Al	4	Zy35	Sm.	Ctr.	69	-4	0	476	145	21.3	8.5 in.	0	0	21.3	
3	A/no Al	4	Zy35	Sm.	Ctr.	57	0	0	738	225	51.2	Yes	597	182	17.7	
4	A/no Al	4	Zy35	Sm.	Ctr.	60	-5	>+3	751	229	53.1	Yes	653	199	13.0	Repeat of 3
5	A w/Al	4	Zy35	Sm.	Ctr.	47	-4	+3	466	142	20.4	4 in.	0	0	20.4	
6	A w/Al	4	Zy35	Sm.	Ctr.	45	-2	0	672	205	42.5	Yes	535	163	15.6	
7	A/no Al	4	Zy35	Sm.	Ctr.	44	0	+5	620	189	36.1	Yes	403	123	20.8	
8	A/no Al	4	Zy35	Sm.	Ctr.	48	-10	>+7	633	193	37.7	10.5 in.	0	0	37.7	Repeat of 7; significant yaw
9	A/no Al	4	Zy35	Sm.	Ctr.	50	-7	>+7	626	191	36.9	10 in.	0	0	36.9	Repeat of 7; significant yaw
10	A/no Al	4	Zy35	Sm.	Ctr.	47	-7	-3	630	192	37.3	Yes	462	141	17.2	Repeat of 7
11	A/no Al	12	Zy35	Lg.	Ctr.	43	0	0	508	155	63.0	12 in.	0	0	63.0	
12	A/no Al	4	Zy35	Lg.	Ctr.	48	-2	+2	502	153	184.3	Yes	380	116	78.4	
13	A/no Al	12	Zy35	Lg.	Ctr.	51	0	0	617	188	92.8	15 in.	0	0	92.8	
14	A/no Al	4	Zy35	Lg.	Ctr.	43	0	0	492	150	177.1	Yes	387	118	67.5	Repeat of 12
15	A w/Al	4	Zy35	Lg.	Ctr.	47	-2	0	505	154	186.7	Yes	377	115	82.6	30-g piece of Al flew off at ≤146 m/s (≤320 J of K.E.)
16	A/no Al	12	Zy35	Lg.	Ctr.	48	0	0	745	227	135.2	Yes	476	145	80.1	
17	A/no Al	12	Zy35	Lg.	Ctr.	48	0	0	751	229	137.6	Yes	495	151	77.8	Repeat of 16
18	A w/Al	12	Zy35	Lg.	Ctr.	51	0	0	735	224	131.7	Yes	489	149	73.4	65-g piece of Al flew off at ≤50 m/s (≤80 J of K.E.)
19	A w/Al	12	Zy35	Lg.	Ctr.	48	0	0	741	226	134.0	Yes	505	154	71.8	Repeat of 18
20	A/no Al	12	Zy35	Sm.	Ctr.	N.A.	N.A.	N.A.	909	277	25.9	9 in.	0	0	25.9	Dust obscures images. Pitch and yaw may be significant.
21	A/no Al	12	Zy35	Lg.	Ctr.	45	0	0	692	211	116.8	Yes	344	105	87.9	
22	A/no Al	12	Zy35	Lg.	Ctr.	49	0	0	699	213	119.1	Yes	343	105	90.4	Repeat of 21
26	A/no Al	12	Zy35	Lg.	Ctr.	6	0	0	672	205	110.0	Yes	558	170	34.3	
27	A/no Al	12	Zy35	Lg.	Ctr.	10	0	0	686	209	114.3	Yes	567	173	36.0	Repeat of 26
28	A/no Al	8	Zy17	Lg.	Ctr.	50	0	0	741	226	141.6	Yes	485	148	80.9	
29	A/no Al	8	Zy17	Lg.	Ctr.	49	0	0	748	228	144.1	Yes	502	153	79.2	Repeat of 28
30	A/no Al	8	Zy17	Lg.	Ctr.	49	0	-2	613	187	96.9	12 in.	0	0	96.9	
31	A/no Al	12	Kev29	Lg.	Ctr.	52	0	0	686	209	116.4	Yes	495	151	55.7	
32	A/no Al	12	Kev29	Lg.	Ctr.	48	0	0	686	209	116.4	Yes	489	149	57.3	Repeat of 31
33	A/no Al	12	Kev29	Lg.	Ctr.	46	0	0	489	149	59.2	12 in.	0	0	59.2	
34	A/no Al	12	E. E. Zy	Lg.	Ctr.	48	0	0	686	209	114.3	Yes	518	158	49.0	
35	A/no Al	12	E. E. Zy	Lg.	Ctr.	54	0	0	689	210	115.4	Yes	541	165	44.2	Repeat of 34
36	A/no Al	12	E. E. Zy	Lg.	Ctr.	49	0	0	443	135	47.7	12 in.	0	0	47.7	

TABLE 2-2. PARAMETERS AND ENERGY ABSORPTION FOR THE BALLISTIC IMPACT TESTS (Continued)

Test No. [a]	Configur-ation [b]	Target		Im-pac-tor [d]	Impact				Impact Velocity		KE/AD[f] (kJ g/cm^2)	Pen.? If not, max. defl. [g]	Residual Velocity		SEA [h] (kJ g/cm^2)	Comments
		No. Plies	Material [c]		Loca-tion	Orientation [e] (°)										
						Roll	Pitch	Yaw	(f/s)	(m/s)			(f/s)	(m/s)		
39	B w/Al	12	Zy35	Lg.	Ctr.	47	0	0	620	189	93.5	15 in.	0	0	93.5	
40	B w/Al	12	Zy35	Lg.	Ctr.	56	0	0	748	228	136.0	Yes	587	179	52.2	
41	B/no Al	12	Zy35	Lg.	Ctr.	49	0	0	741	226	133.6	Yes	341	104	105.3	Repeat of 40 w/o Al
42	B w/Al	12	Zy35	Lg.	Ctr.	51	0	0	748	228	136.0	Yes	567	173	57.7	Repeat of 40
44	B/no Al	12	Zy35	Lg.	Ctr.	51	0	0	751	229	137.2	19 in.	0	0	137.2	Repeat of 41; 3 out of 4 side pegs tore through to fabric edge on most plies.
45	B w/Al	12	Zy35	Lg.	Ctr.	58	0	0	748	228	136.0	Yes	594	181	50.3	Repeat of 42
46	B/no Al	4	Zy35	Sm.	Ctr.	48	0	0	620	189	35.7	12 in.	0	0	35.7	Repeat of 43
47	B w/Al	4	Zy35	Sm.	Ctr.	67	-5	-2	649	198	39.2	Yes	469	143	18.8	
48	B w/Al	4	Zy35	Sm.	Ctr.	53	-5	3	653	199	39.6	Yes	479	146	18.3	Repeat of 47
49	B/no Al	4	Zy35	Sm.	Ctr.	49	-15	8	787	240	57.6	Yes	633	193	20.4	
50	B w/Al	4	Zy35	Sm.	Ctr.	48	0	0	528	161	25.9	6 in.	0	0	25.9	
51	B/no Al	4	Zy35	Sm.	Ctr.	56	-7	-2	807	246	60.5	Yes	702	214	14.7	Repeat of 49
52	B/no Al	12	Zy35	Lg.	O. C.	49	0	0	754	230	138.4	Yes	469	143	84.9	Impact 12.3 in. l.o.c.
53	B/no Al	12	Zy35	Lg.	O. C.	48	-2	0	741	226	133.6	Yes	384	117	97.8	12.3 in. l.o.c., 6 in. below. Peg nearest impact tore to fabric edge on last 9 plies.
54	B/no Al	4	Zy35	Sm.	O. C.	48	-2	-2	613	187	35.0	9 in.	0	0	35.0	12.3 in. l.o.c., 6 in. below.
55	B/no Al	12	Zy35	Lg.	O. C.	49	-2	0	748	228	136.0	Yes	492	150	77.1	12.3 in. l.o.c., 6 in. below. Repeat of 53.
56	B/no Al	4	Zy35	Sm.	O. C.	48	-6	-7	761	232	53.8	Yes	604	184	20.0	12.3 in. l.o.c., 6 in. below.
58	A/no Al	4	Zy35	Sm.	O. C.	54	-3	3	630	192	36.9	Yes	485	148	15.0	9.0 in. l.o.c., 3.3 in. down
59	A/no Al	4	Zy35	Sm.	O. C.	48	-5	0	643	196	38.4	Yes	495	151	15.6	Repeat of 58
60	A/no Al	4	Zy35	Sm.	Ctr.	90	0	-3	643	196	38.4	10.5 in.	0	0	38.4	
61	A/no Al	4	Zy35	Sm.	Ctr.	88	0	8	636	194	37.6	Yes	341	104	26.8	Repeat of 60, but warp and fill directions were reversed.
62	A/no Al	4	Zy35	Sm.	Ctr.	11	0	0	626	191	36.5	9 in.	0	0	36.5	

[a] Includes only those tests with complete energy absorption data and no premature loading of the fabric.

[b] A—rigid ladder frame configuration; with aluminum has 0.229-cm- (0.09-in.)-thick Al 2024-T3 backplate. B—96.5-cm- (38-in.)-square configuration; with aluminum has 0.05-in.-thick Al 2024-T3 backplate, with field bolts.

[c] Zy35—-baseline (500 Denier); Zy17 (1500 Denier); Kev29 (600 Denier); and E. E. (environmentally exposed) Zy—baseline Zylon exposed to high temperatures and humidities at Boeing.

[d] Sm. is the 5.08- x 5.08- x 0.635-cm- (2- x 2- x 1/4-in.) impactor, weighing 126-128 g (0.28lb); Lg. is the 10.16- x 10.16- x 1.27-cm (4- x 4- x 1/2-in.) impactor, weighing 989-992 g (2.18-2.19 lb). Both are tool steel rectangular parallelopipeds, with edges rounded to a radius of ≈0.015 in.

[e] 0° roll means the longer edge of the impact end of the impactor is in the vertical direction. Pitch and yaw are based on lab coordinates and denote change in vertical and horizontal angle, respectively, of the impactor's original axial direction.

[f] The impact kinetic energy divided by the areal density of the fabric target.

[g] Maximum deflection of the fabric in the direction of impact.

[h] SEA (specific energy absorbed) is the energy absorbed divided by the fabric areal density.

l.o.c. = left of center

K.E. = Kinetic energy

The high-speed video camera records of the tests were provided to the program team. Selected photographs from three of the video camera records are shown in figures 2-9 through 2-11, as examples of the type of data obtained. Figure 2-9 shows a small impactor penetrating the fabric barrier, figure 2-10 shows a large impactor being stopped by the barrier, and figure 2-11 shows a large impactor penetrating the fabric barrier with an aluminum backing sheet.

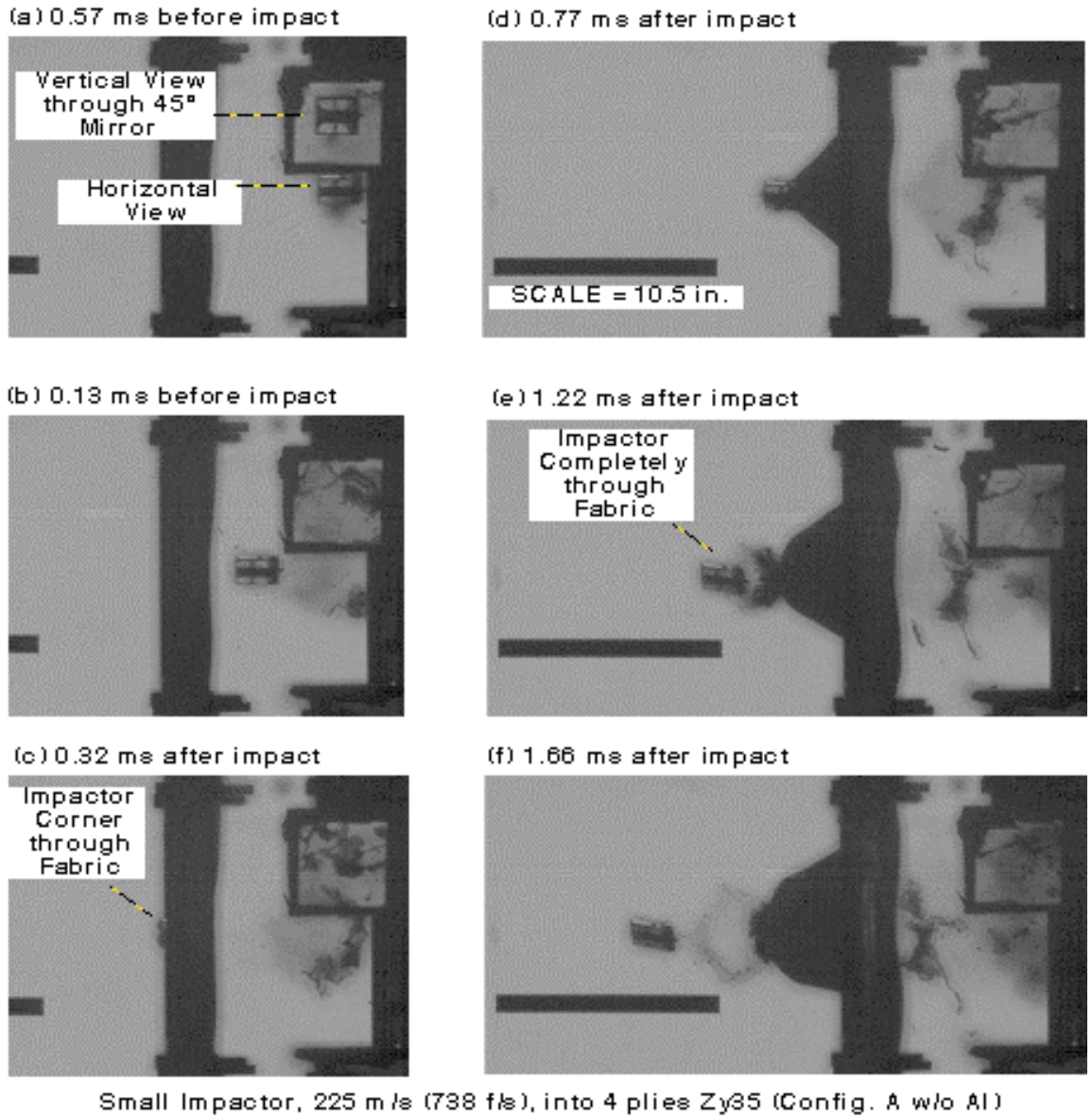

FIGURE 2-9. SELECTED VIDEO CAMERA FRAMES FROM TEST 3

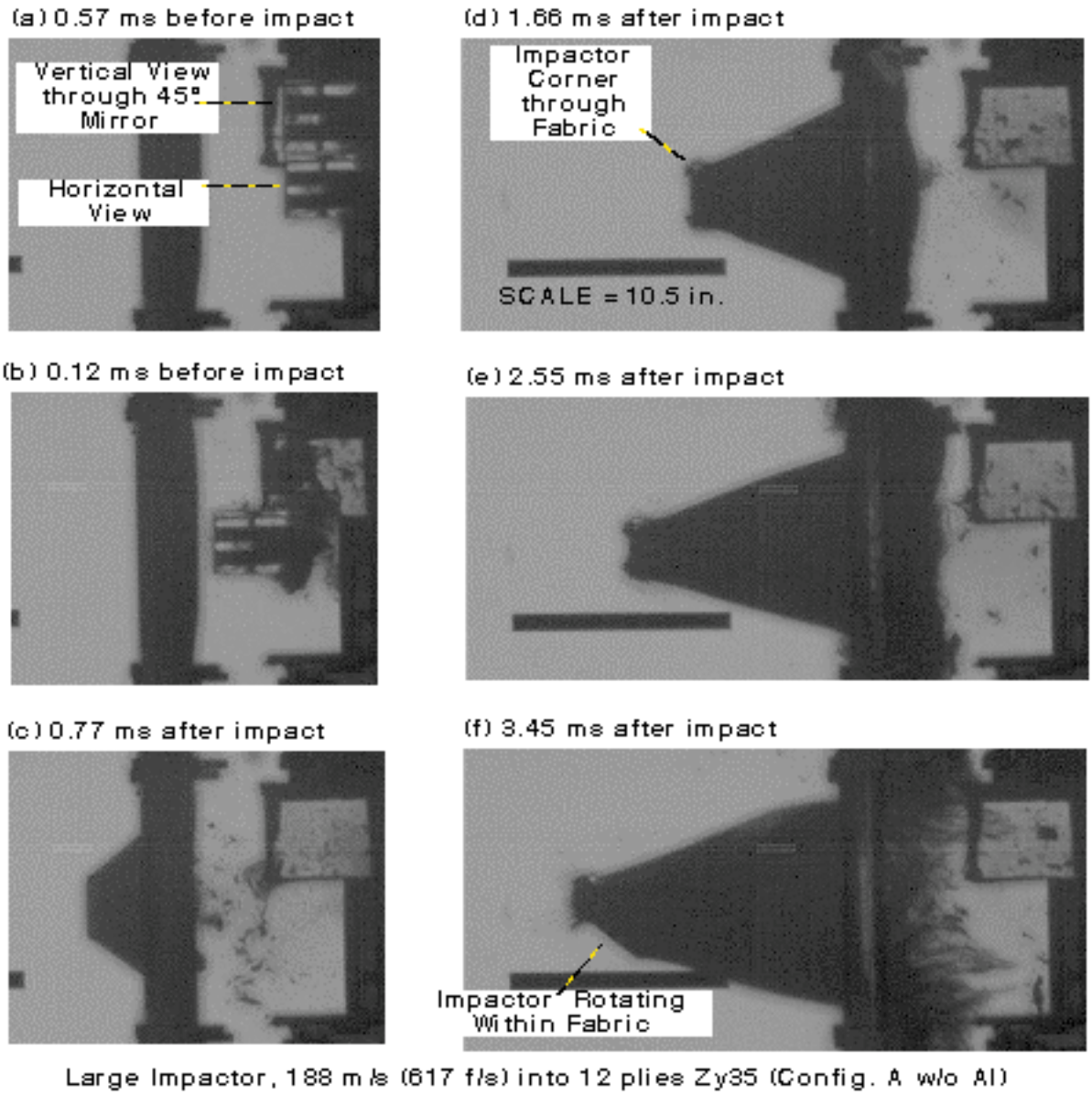

FIGURE 2-10. SELECTED VIDEO CAMERA FRAMES FROM TEST 13

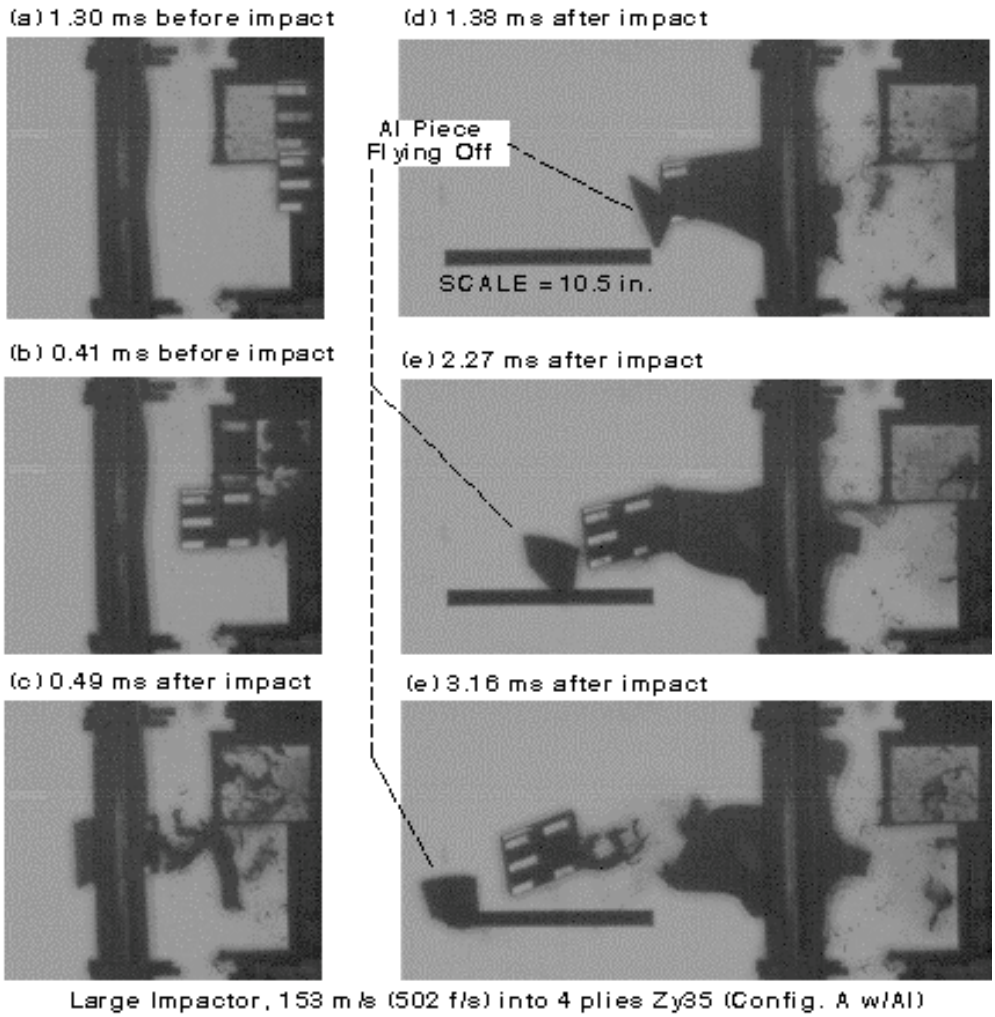

FIGURE 2-11. SELECTED VIDEO CAMERA FRAMES FROM TEST 15

The impact velocity and the residual velocity of the impactor were determined from the video camera records along with the preimpact orientation of the impactor and the maximum deflection of the fabric for the nonpenetration case. Energy absorption values were determined by subtracting the residual kinetic energy of the impactor (zero for the nonpenetration case) from the impact kinetic energy. The specific energy absorbed (SEA), which is used as the figure of merit for comparison of various fabric barriers, is calculated by dividing the energy absorbed by the areal density of the fabric.

2.2.1 Test Repeatability.

The preimpact orientations of the impactor are given in table 2-2. The average deviations of the actual impact orientations from the intended orientations were:

	Roll	Pitch	Yaw
Large Impactor	5°	<1°	<1°
Small Impactor	7°	4°	>3°

The deviations in the roll appeared to be from rotations of the sabot within the barrel, something that is not expected but also not controllable. Although the large impactors experienced negligible variation in yaw and pitch, the small impactors varied in yaw and pitch, probably from nonuniformities in release from the sabot, exacerbated by having to break through the Mylar diaphragm. Nevertheless, the impactor orientation variations were small compared to typical impact tests with similar impactors.

Figure 2-12 shows a graph of residual velocity versus impact velocity for all of the repeat tests that resulted in full penetration.* Repeat tests are enclosed within the same border (usually a rounded-corner rectangle). Impact velocities are very repeatable—they are within or very nearly within the ±1% measurement uncertainties for all repeat tests. Residual velocities are also very close (≤ ±2%) for repeat tests with the large impactors, which means that there is very little variability in fabric barrier response for identical test parameters. For the small impactors, the residual velocities are not quite as close (variability of ≤ ±4% for repeat tests), probably due to the larger variation in the impact orientation.

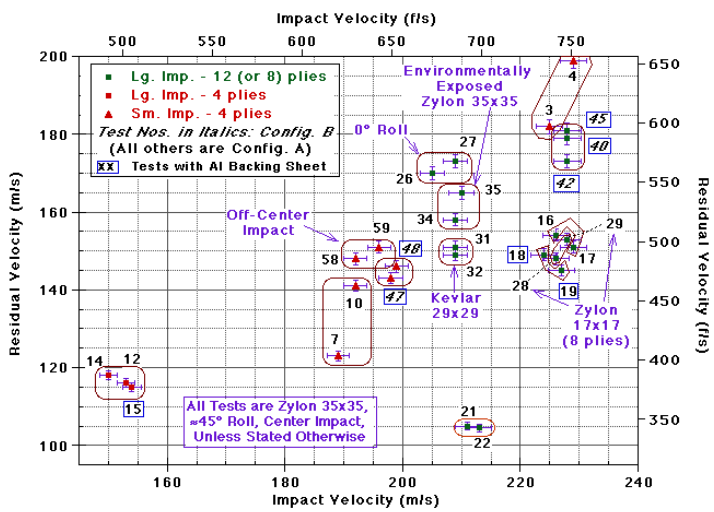

FIGURE 2-12. RESIDUAL VELOCITY VERSUS IMPACT VELOCITY DATA FOR REPEAT TESTS WITH FULL PENETRATION

2.2.2 Comparison of Fabric Materials.

To compare the ballistic effectiveness of the different fabric barrier materials, a test series was performed in which the fabric material was the only variable. The tests conditions were:

- Configuration A, without an aluminum backing sheet.
- Large impactor at ≈45° roll, with impact at target center.
- Thicker target barrier (12 plies of Zy35 or Kev29, or 8 plies of Zy17).

* The only repeat tests not included in this graph involve two pairs of which one of the two tests resulted in the fabric tearing off one or more of the pegs, significantly increasing the energy absorbed.

The SEA results (as shown in figure 2-13) are as follows:

- The baseline Zy35 (500-Denier yarns) and the heavy Zy17 (1500-Denier yarns) behaved the same, absorbing 78-97 kJ/g/cm^3 (28-35 kft-lb/lb/ft^3).

- The Kev29 (600-Denier yarns) was only about two-thirds as effective as the baseline material, absorbing 56-59 kJ/g/cm^3 (20-21 kft-lb/lb/ft^3).

- The E.E. Zy35 (exposed to 160°F and 85% humidity for 3 weeks) was only about half as effective as the baseline material, absorbing 44-49 kJ/g/cm^3 (16-18 kft-lb/lb/ft^3).

The results of these material variation tests were as expected. Previous smaller-scale ballistics tests performed at SRI had shown Kevlar to be weaker than Zylon [1], and data from the Toyobo, Company (the manufacturer of Zylon) had shown significant decrease in the strength of Zylon yarns subjected to high-temperature, high-humidity environments similar to that of the E.E. Zylon [2].

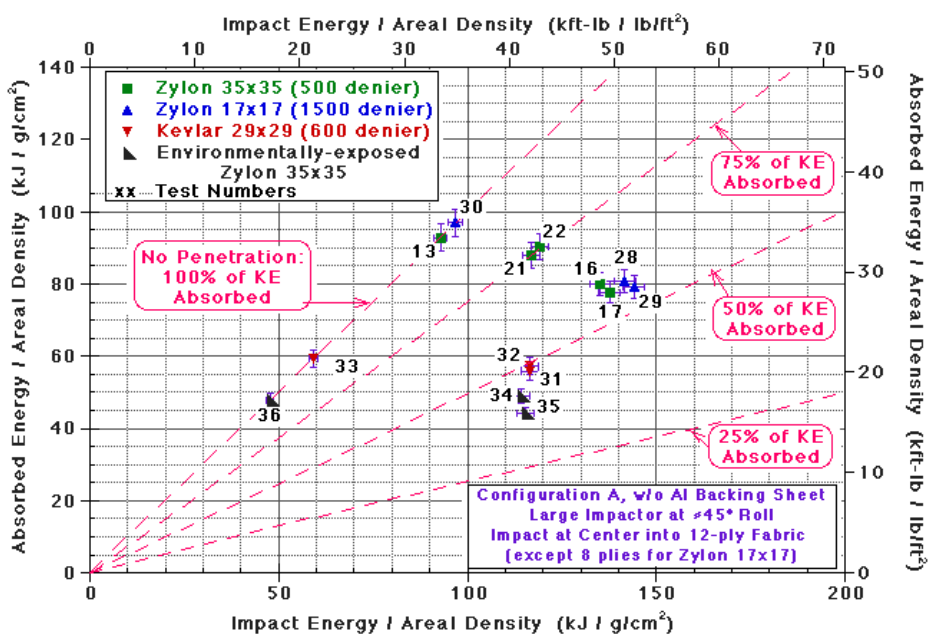

FIGURE 2-13. ENERGY ABSORPTION RESULTS FOR VARIOUS FABRIC MATERIALS

Based on previous smaller-scale ballistics tests performed at SRI [3], which had shown similar ballistic results for Zylon fabrics of different areal densities, it was expected that the baseline Zy35 and heavy Zy17 materials would behave similarly, and they did. However, all the previous tests involved Zylon fabrics with different yarn counts, but the same 500-Denier yarns. The current tests were SRI's first ballistic tests with the 1500-Denier yarns. It should be noted that these results did not match the results of the fabric ring impact tests performed recently at NASA under another FAA program in which the Zy17 significantly outperformed the Zy35 in tests with a very different fabric gripping geometry and projectile.

2.2.3 Zy35 Results for Configuration A.

The results for all Configuration A tests with the baseline Zy35 material are shown in figure 2-14, while a higher-resolution graph (figure 2-15) allows easier interpretation of the results for those tests with the small impactor. Most of these tests had center impacts, with close to 45° roll, but there were a few tests with ≈0° or ≈90° roll (both small and large impactors) and a couple of tests with off-center impacts (small impactor only).

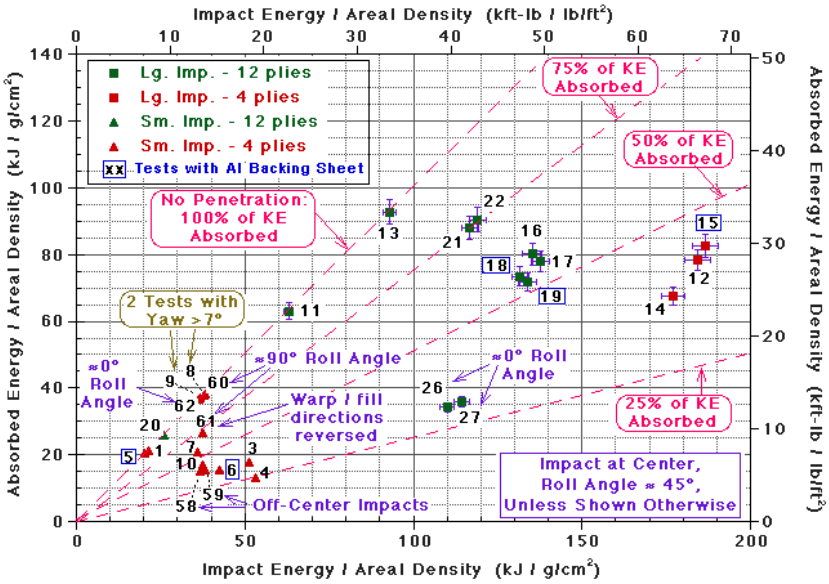

FIGURE 2-14. ENERGY ABSORPTION RESULTS FOR Zy35 CONFIGURATION A TESTS

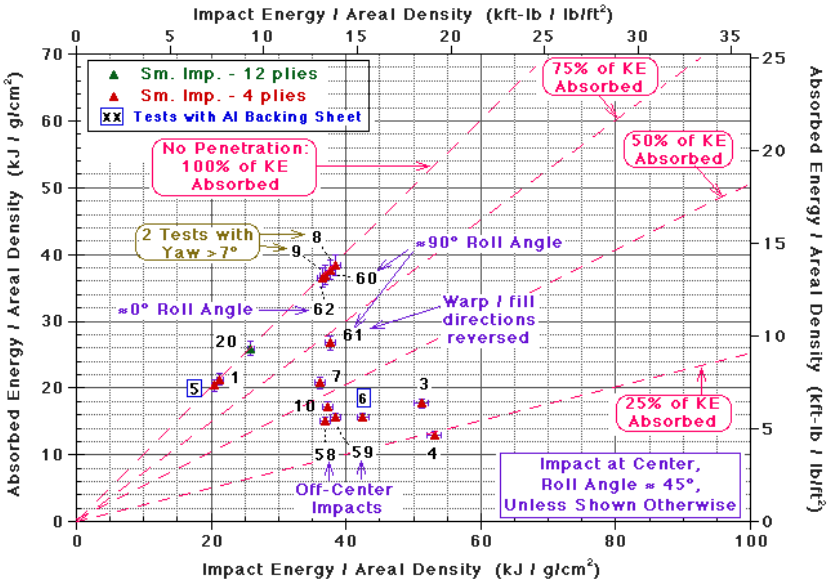

FIGURE 2-15. ENERGY ABSORPTION RESULTS FOR Zy35 CONFIGURATION A TESTS WITH THE SMALL IMPACTOR

The presence or absence of the 0.229-cm- (0.090-in.)-thick aluminum 2024-T3 backing sheet had negligible effect on the ballistic efficiency of the fabric barrier for Configuration A tests. A comparison of tests with the backing sheet and identical tests without the backing sheet (e.g., tests 5 versus 1, 18 and 19 versus 16 and 17, 15 versus 12 and 14, and 6 versus 7 and 10) showed little or no change in the energy absorbed. This was true despite the large amount of deformation and damage, which occurred in tests with the aluminum backing sheet. The damage occurred mostly in the form of petaling (see figure 2-16), but occasionally small pieces of aluminum, with a small fraction of the total residual kinetic energy, were separated from the backing sheet by the impact (see figure 2-11).

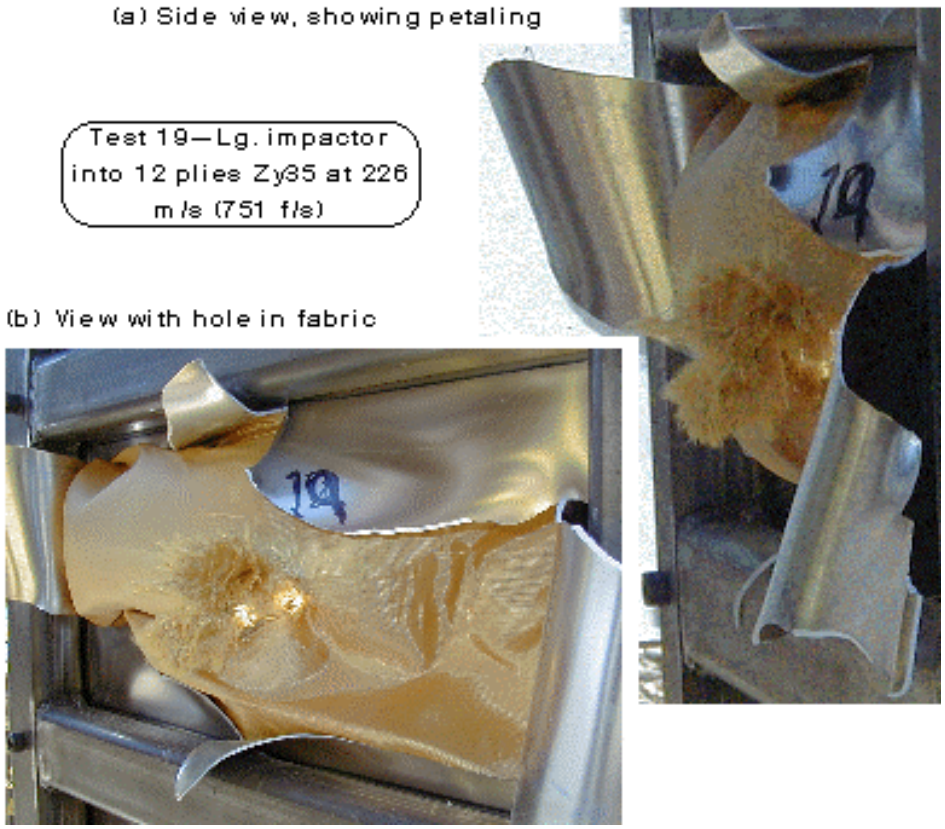

FIGURE 2-16. VIEWS OF DAMAGE TO ALUMINUM BACKING SHEET FROM CONFIGURATION A TEST

For large impactor, center impact, close to 45° roll tests, resulting in full penetration of the Zy35 fabric barrier (tests 12, 14 through 19, 21, and 22), SEAs were in the range of 80 ±13 kJ/g/cm^2 (28 ±4 kft-lb/lb/ft^2), with the values slightly rising as the ballistic limit was approached. For close to 0° roll tests with the large impactors (tests 26 and 27), SEAs were reduced to 35 kJ/g/cm^2 (12.5 kft-lb/lb/ft^2). This decrease in SEA was expected because an impactor at 0° roll needs to break through fewer yarns to penetrate than an impactor at a 45° roll. However, the ≈60% decrease in the SEA was much greater than the ≈30% decrease in the number of directly impacted yarns.

For small impactor, center impact, close to 45° roll tests, resulting in full penetration of Zy35 (tests 3, 4, 6, 7, and 10), SEAs were in the range of 17 ±4 kJ/g/cm^2 (6 ±1.5 kft-lb/lb/ft^2), with the values also rising slightly as the ballistic limit was approached.

Two small impactor tests with the same impact velocity as tests 6 and 7, but with significant (>7°) yaws (tests 8 and 9), had significantly higher SEAs—≈37 kJ/g/cm^2 (≈13 kft-lb/lb/ft^2) and in fact were stopped by the fabric barrier, as were a couple of tests (tests 60 and 62) with either ≈0° or ≈90° roll. Another test with ≈90° roll, but with the warp and fill fabric directions on the target reversed (test 61), had an SEA midway between the others—27 kJ/g/cm^2 (≈10 kft-lb/lb/ft^2).

Clearly, the orientation angle had a large effect on the energy absorption. Tests with large yaw had higher energy absorption, possibly because the large yaw forces the impactor to break through more yarns in order to penetrate. The yaw could also have enabled the impactor to be turned more easily before penetration. However, the ≈0° roll and ≈90° roll small impactor tests, which were expected to have a lower SEA than the ≈45° roll tests, had a larger SEA in this study. It is possible that yaw affected these results, but because of the limited amount of tests at 0 and 90° roll, it could not be determined if this was consistent.

The two off-center impacts (tests 58 and 59, with the small impactor centered 3.2 in. from the nearest peg) had slightly lower SEA than the center impact tests.

2.2.4 Zy35 Results for Configuration B.

The results for the Configuration B tests with the baseline Zy35 material are shown in figure 2-17. All these tests had ≈45° roll; most had center impacts, but there were a few off-center impacts.

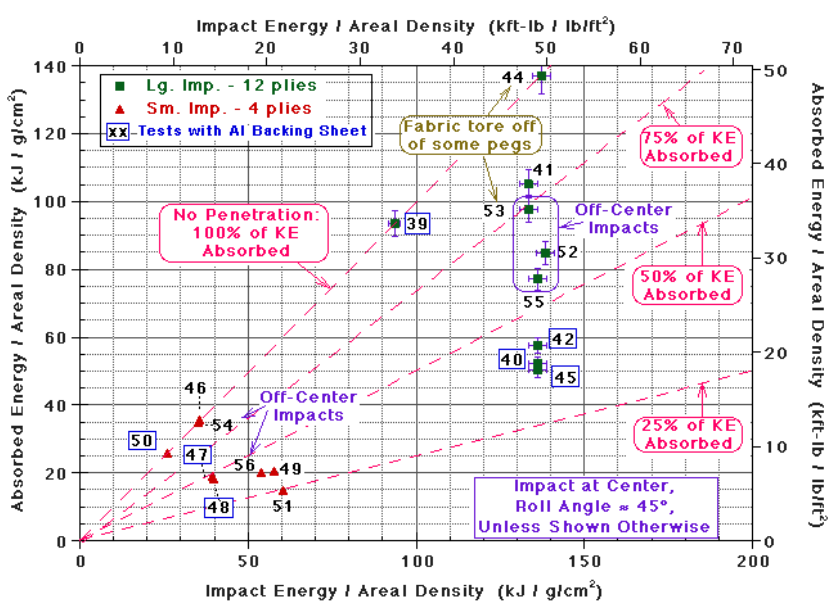

FIGURE 2-17. ENERGY ABSORPTION RESULTS FOR Zy35 CONFIGURATION B TESTS

For the Configuration B tests, the presence of the 0.127-cm- (0.050-in.)-thick aluminum 2024-T3 backing sheet with the field bolts (small #10-24 bolts similar to ones that might be used in the field to hold the fabric in place) had a significant negative effect on the ballistic efficiency of the fabric barrier, particularly for the large impactors. The SEA for a large impactor, center impact, close to 45° roll test without the aluminum backing sheet (test 41) was 105 kJ/g/cm^2 (38 kft-lb/lb/ft^2), while for similar tests with the aluminum plate (tests 40, 42, and 45), the SEAs were only ≈53 kJ/g/cm^2 (≈19 kft-lb/lb/ft^2), a reduction of 50%. Small impactor tests with the backing sheet (tests 47 and 48) also showed a decrease in SEA compared to similar tests without the backing sheet (tests 49, 51, 54, and 56), but the decrease was less substantial than for the large impactors (possibly affected by larger variations in the impact yaw and pitch).

The added constraint of the field bolts on the deformation of the fabric barrier is the most likely cause for this large deleterious effect of the 0.127-cm- (0.050-in.)-thick aluminum backing sheet on the SEA in the Configuration B tests, particularly since the presence of a thicker (0.229-cm-(0.090-in.) -thick) aluminum backing sheet, with no field bolts, was shown to have no effect on the SEA in the Configuration A tests. The field bolts were so strong that the deforming fabric tugging on the field bolts caused them to tear through the aluminum backing sheet for distances of up to 4 in. from the field bolts.

Figures 2-18 through 2-21 present various Configuration B tests with the aluminum backing sheet, showing the deformation and petaling failure and the tearing of the aluminum caused by the field bolts.

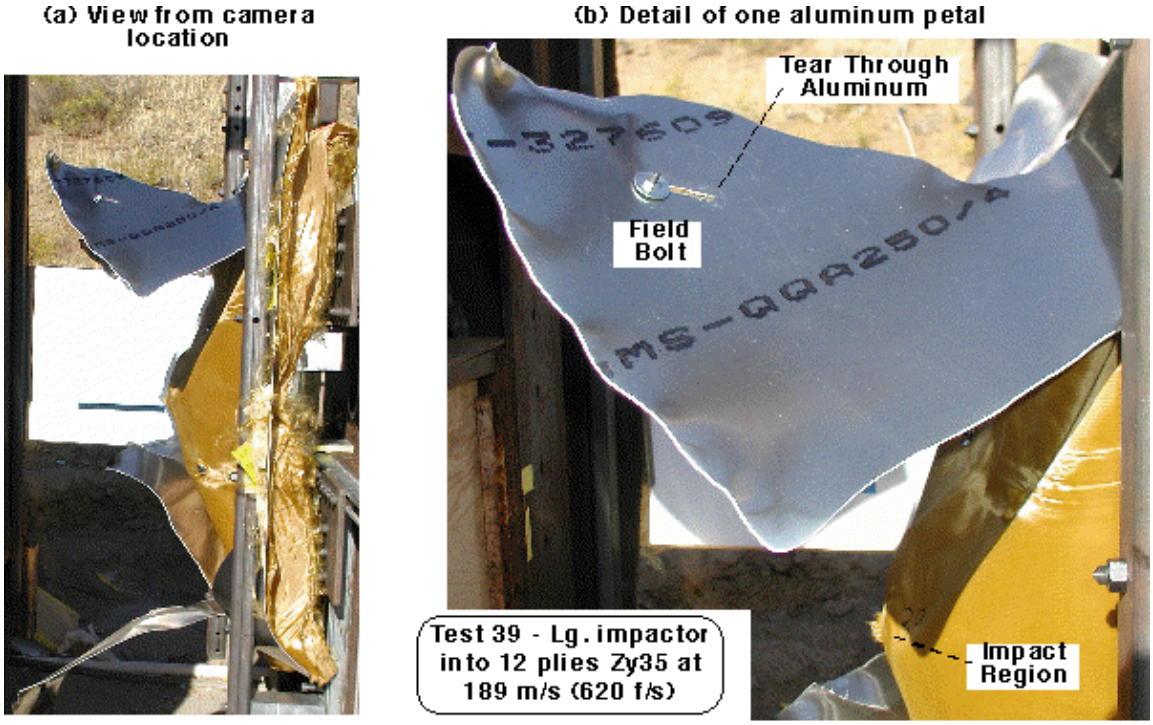

FIGURE 2-18. VIEWS OF TARGET AFTER CONFIGURATION B TEST 39 (WITH NO PENETRATION)

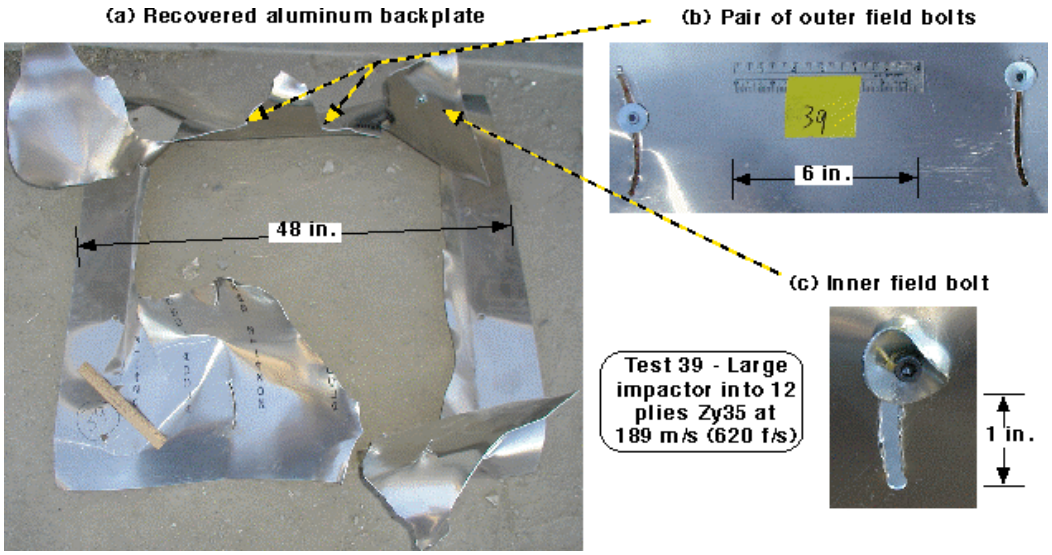

FIGURE 2-19. VIEWS OF ALUMINUM BACKING SHEET AFTER CONFIGURATION B TEST 39

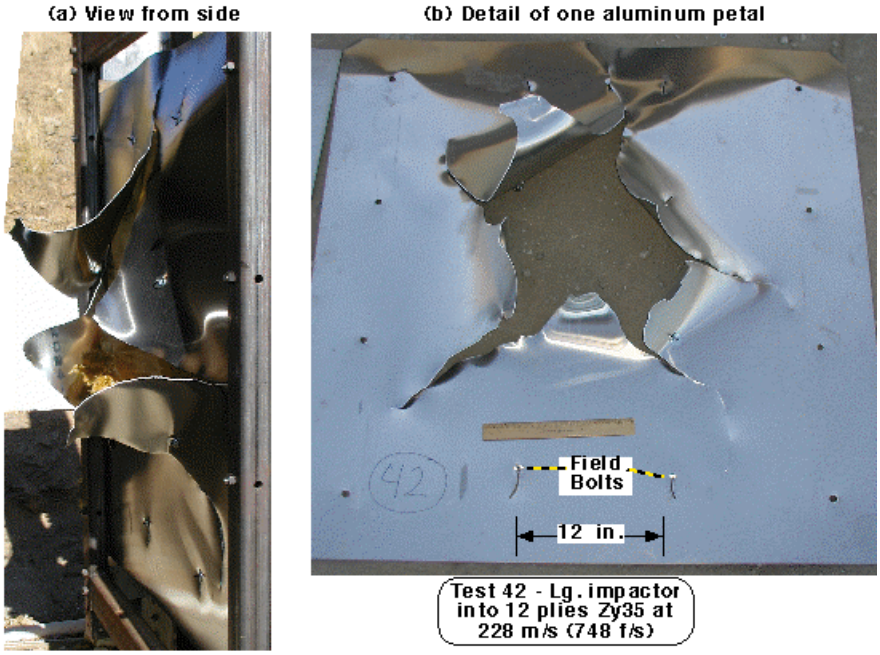

FIGURE 2-20. VIEWS OF ALUMINUM BACKING SHEET AFTER CONFIGURATION B TEST 42 (COMPLETE PENETRATION)

For Configuration B (with no aluminum backing sheet) off-center impact tests (with impact centers located either 23.4 or 16.5 cm (9.2 or 6.5-in.) away from the nearest peg), the SEAs for tests with the large impactor (tests 52 and 55) were 20%-23% lower than the center impact test (test 41)—the closer to the peg, the lower the SEA. For off-center tests with the small impactor (tests 54 and 56), the SEAs were about the same as the center impact tests.

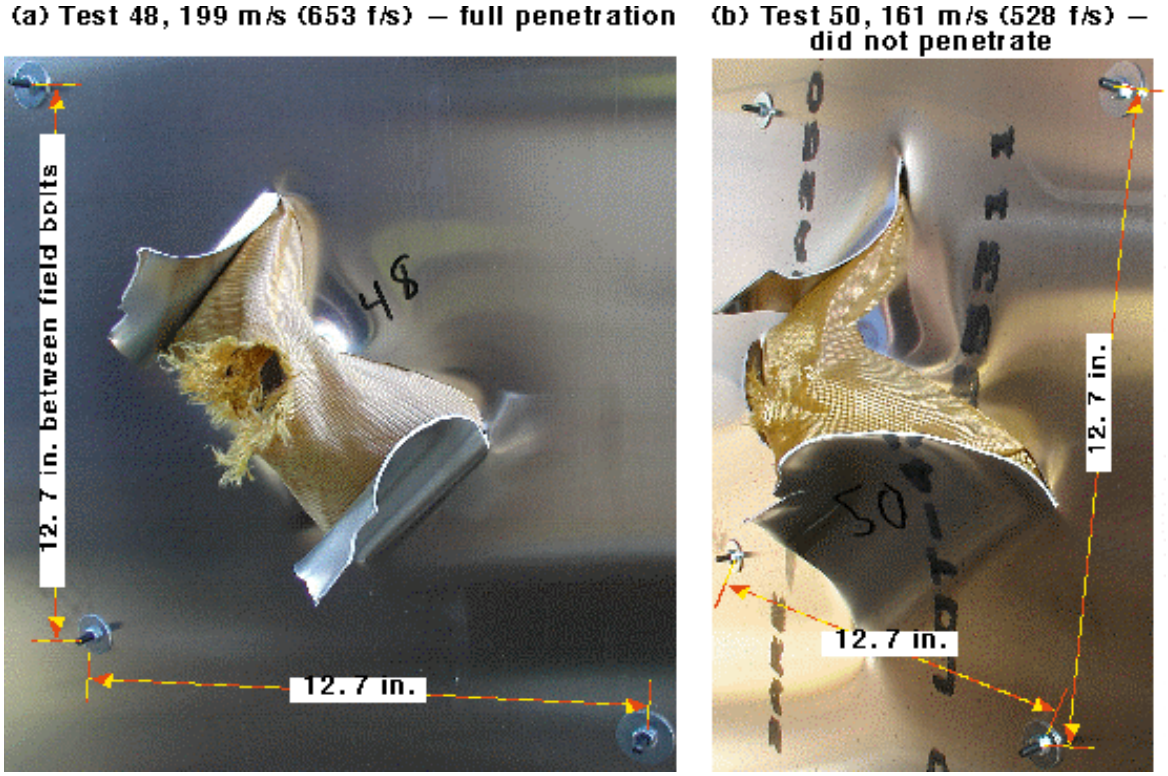

FIGURE 2-21. POSTTEST VIEWS OF ALUMINUM BACKING SHEETS FROM SMALL IMPACTOR CONFIGURATION B TESTS

2.2.5 Fabric Tear-Off From Pegs.

Two close to 45° roll, large impactor tests with Configuration B (no aluminum backing sheet) resulted in fabric plies tearing completely away from one or more of the side pegs, with a significant increase in the SEA, compared to similar tests in which no tear off occurred. These tests (as shown in figure 2-17) were

- Test 53 (off-center impact), in which most of the plies tore off the peg closest to the impact point, yielded an SEA of 98 kJ/g/cm^2 (35 kft-lb/lb/ft^2)—27% higher than test 55, for which there was no fabric tear off.

- Test 44 (center impact), in which most or all plies tore away from three of the four side pegs, yielded an SEA of 137 kJ/g/cm^2 (49 kft-lb/lb/ft^2)—30% higher than test 41, for which there was no fabric tear off.

Figure 2-22 shows the fabric targets recovered from these tests, and the large amount of tearing at the pegs. Fabric tear off from one or more of the side pegs appeared to increase tearing lengths at the remaining side pegs and at all corner pegs, resulting in additional energy absorption, but at the cost of larger fabric deflections.

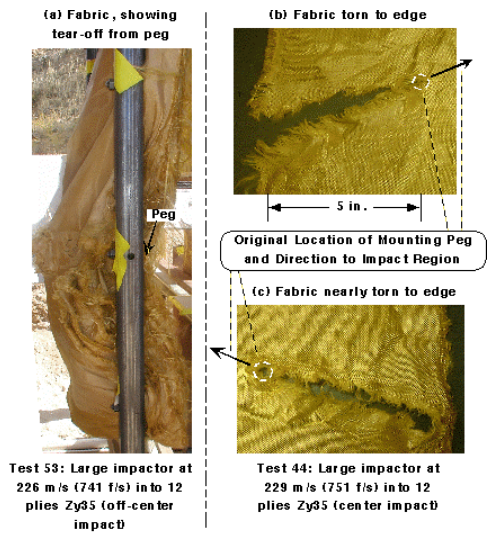

FIGURE 2-22. FABRIC AFTER TEAR OFF FROM PEGS IN TWO CONFIGURATION B TESTS WITHOUT ALIMINUM BACKING SHEET

2.2.6 Comparison of Zy35 Results for Configurations A and B.

A comparison of the results for Configurations A and B is shown in figure 2-23, showing the close to 45° roll, center impact tests with the baseline Zy35 fabric and no aluminum backing sheet, which resulted in full penetration. The SEAs for Configuration B were higher than Configuration A by about 30% for the large impactors (compare test 41 with tests 16 and 17), and by a smaller amount for the small impactors (compare test 49 and 51 with tests 3 and 4). This was as expected because of the larger fabric sheets used in Configuration A and the longer distance from the impact region to the pegs.

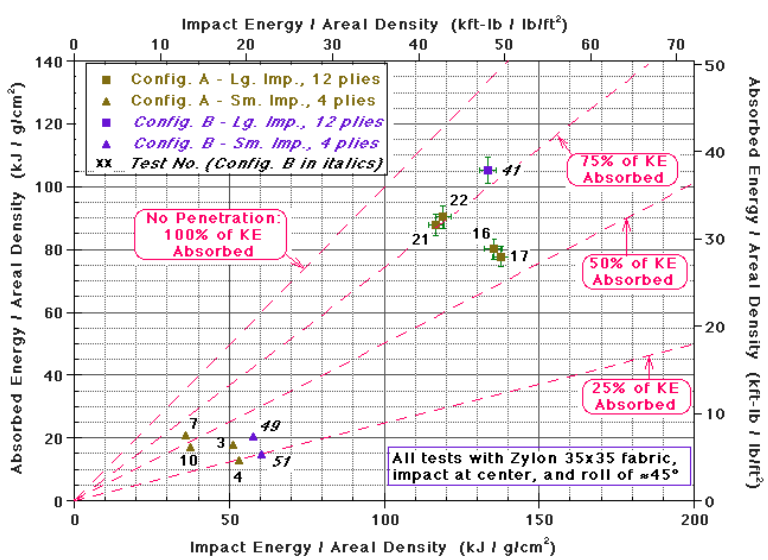

FIGURE 2-23. COMPARISON OF ENERGY ABSORPTION RESULTS FOR CONFIGURATIONS A AND B WITHOUT ALUMINUM BACKING SHEET

2.2.7 Fabric Barrier Damage.

Tearing damage to the fabric plies in the ballistic impact tests occurred in the form of broken yarns in two regions—the impact area and around the pegs. Quantitative data on the tearing damage in those regions, plus data on the tearing of both the fabric and the aluminum at the field bolts for Configuration B tests with the aluminum backing sheet, is shown in table 2-3.

TABLE 2-3. FABRIC DAMAGE IN BALLISTIC IMPACT TESTS

Test No.	For Tests with No Penetration, Damage near Impact Region [ply no.] Length (in.) of residual ligament (or tear-T)[a]	Tear Length at Pegs[b] (in., min. - max.)		Tear Length at Field Bolts[c] (in., min.-max.)			
				Fabric		Aluminum	
		Side	Corner	Inner	Outer	Inner	Outer
1	[1] 1.5, [2-4] negligible	0.5-0.75	0.25-0.5	——	——		
3	——	Neg.-0.5	Neg.-0.25	——	——	——	——
4	——	0.25	Neg.	——	——	——	——
5	[1-4] 0.75	Neg.-0.25	Neg.	——	——	——	——
6	——	Neg.	Neg.	——	——	——	——
7	——	0.5	0.25-0.5	——	——	——	——
8	[1]2.25T, [2,3]1.75T, [4]1.5T	1.0	0.75-1.0	——	——	——	——
9	[1]0.4, [2]0.5, [3,4]0.75	1.0-1.25	1.0-1.25	——	——	——	——
10	——	0.25-0.5	0.25-0.5	——	——	——	——
11	[1-7]3.2-3.5, [8-12] neg.	2.0-2.5	1.5-3.0	——	——	——	——
12	——	2.0-2.5	2.0-3.0	——	——	——	——
13	[1]0.4, [2]0.75, [4-12]≈1	3.0-4.0	3.5-3.75	——	——	——	——
14	——	2.0-3.0	2.25-3.0	——	——	——	——
15	——	0.5-1.25	0.75-1.5	——	——	——	——
16	——	2.25-3.25	2.0-2.5	——	——	——	——
17	——	2.5-3.5	1.5-2.5	——	——	——	——
18	——	1.25-2.5	1.0-1.75	——	——	——	——
19	——	1.25-2.25	1.0-2.0	——	——	——	——
20	[1]2T, [2]0.1, [3-6]0.4-0.8, [7-11]1-1.5, [12]0.5T	0.75-1.5	0.75-1.5	——	——	——	——
21	——	2.5-3.5	2.25-3.25	——	——	——	——
22	——	2.5-3.75	2.25-3.0	——	——	——	——
26	——	0.5-1.0	0.75-1.0	——	——	——	——
27	——	0.25-1.0	0.5-1.25	——	——	——	——
28	——	0.5-1.75	0.5-2.25	——	——	——	——
29	——	0.5-1.25	0.5-2.0	——	——	——	——
30	[1]1.25, [2-5]2-2.25, [6-8]2.5	1.5-2.5	1.25-2.5	——	——	——	——
31	——	1.0-1.5	0.5-4.5	——	——	——	——
32	——	0.75-1.75	0.5-5.0	——	——	——	——
33	[1]1.5, [2-6]2.5, [7-12]2.75	1.75-3.0	1.25-3.5	——	——	——	——
34	——	1.0-2.0	1.5-2.5	——	——	——	——
35	——	0.5-1.5	1.0-1.75	——	——	——	——
36	[1[2.5, [2-6]2.75-3.25, [7-12]0.5-0.25T	1.5-2.25	1.5-2.5	——	——	——	——

TABLE 2-3. FABRIC DAMAGE IN BALLISTIC IMPACT TESTS (Continued)

Test No.	For Tests with No Penetration, Damage near Impact Region [ply no.] Length (in.) of residual ligament (or tear-T)[a]	Tear Length at Pegs[b] (in., min. - max.)		Tear Length at Field Bolts[c] (in., min.-max.)			
				Fabric		Aluminum	
		Side	Corner	Inner	Outer	Inner	Outer
39	[1]1, [2-8]1.75-3 ,[9-12]1T	1.5-2.5	0.5-.075	0.25-1.25	Neg.-1.0	≈1.25	≈4
40	——	0.5-0.75	0.25-0.75	Neg.-0.5	Neg.-0.75	0.5	0.5
41	——	2.0-4.5	1.25-3.0	——	——	——	——
42	——	0.75-1.25	0.25-0.75	0.5-1.0	0.25-0.75	Neg.-0.5	0.5-1.25
44	[1] Tot. Pen., [2-3]<0.25, [4]0.5, [5-9]1-1.5, [9-12]2-2.5	4.0-5.5	1.5-3.5	——	——	——	——
45	——	0.25-1.0	Neg.-0.5	Neg.-0.5	Neg.-0.5	0.5-0.75	1.0-1.75
46	[1]1.25,[2-3]1.5,[4]1.75	1.0-1.5	0.25-1.25	——	——	——	——
47	——	0.25	Neg.-0.5	Neg.	Neg.	Neg.	Neg.
48	——	Neg.-0.5	Neg.-0.5	Neg.-0.25	Neg.-0.25	Neg.	Neg.
49	——	0.25-.05	0.25-0.5	——	——	——	——
50	[1]1.0,[2-4]1.25	0.25-0.5	0.25	Neg.-0.5	Neg.-0.5	Neg.	Neg.
51	——	0.25-0.75	.025-.075	——	——	——	——
52	——	0.5-3.75	0.25-3.0	——	——	——	——
53	——	0.25-5.5	0.75-4.5	——	——	——	——
54	[1]0.5,[2-5]1.0	0.25-3.5	0.25-0.75	——	——	——	——
55	——	0.25-5.0	0.25-2.5	——	——	——	——
56	——	Neg.-1.0	Neg.-0.75	——	——	——	——
58	——	Neg.-0.25	Neg.-0.75	——	——	——	——
59	——	Neg.-0.5	Neg.-0.5	——	——	——	——
60	[1]1.5T,[2-3]1.0T,[4]0.75T	0.25-1.75	0.75-1.5	——	——	——	——
61	——	0.5-1.0	0.25-1.0	——	——	——	——
62	——	0.5-1.5	0.5-1.5	——	——	——	——

[a] In most no-penetration tests, two impactor corners perforated the fabric, leaving a residual ligament between them. In some tests, one corner perforated the fabric, leaving a single tear (T).

[b] Length (along the diagonal) of the fabric tears at the pegs. Side pegs are the four closest to point of impact; corner pegs are the four more distant. Neg. denotes < 1/8 in.

[c] For Configuration B with aluminum, tearing in the fabric and the aluminum backplate at the field bolt locations. Inner bolts are the four closest to point of impact; outer are the four more distant. Neg. denotes < 1/8 in.

The front corners of the impactors perforated the fabric first, often shortly after impact, before the fabric had deformed significantly (see figure 2-9(c)). Even if the fabric prevented penetration, the impactor's corners usually perforated all the fabric plies (see figures 10(d) through 10(f)), but a ligament of the fabric remained in position in front of the impactor. The length of this remaining ligament, as determined from examination of the recovered specimens, monotonically increased with the ply number (the first ply impacted is no. 1, etc.), as shown in table 2-3.

For tests with a lower SEA, in which the impactor penetrated easily (i.e., had a relatively small fraction of its energy absorbed by the fabric during penetration), the yarns tore along the region of contact with the impactor, and there was relatively little tearing at the pegs.

For tests with a higher SEA, in which the impactor had a large fraction of its energy absorbed during penetration, failure in the fabric did not necessarily occur along the region of contact with the impactor. As shown in figure 2-24, the yarns failed along the perimeter of a rectangle whose opposite corners are located at the edges of the impactor's front corners. This remote type of yarn failure, which occurs from loading by the intersecting perpendicular yarns rather than loading directly by the impactor, was observed in various other fabric failure scenarios [4].

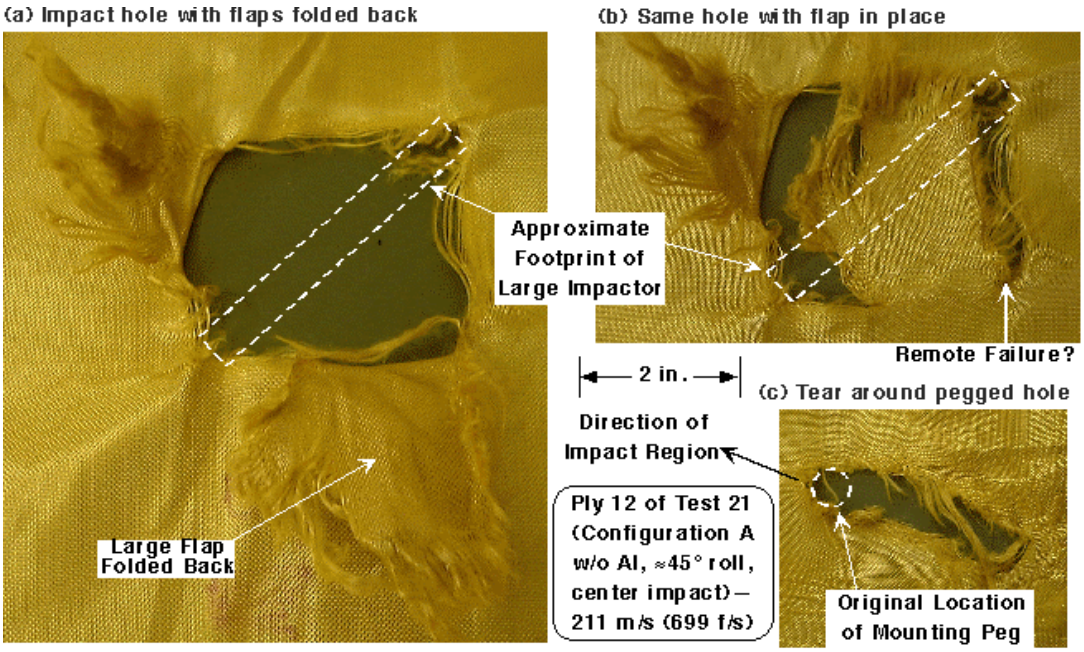

FIGURE 2-24. TYPICAL DAMAGE TO Zy35 FABRIC IN IMPACT AND PEGGED AREAS FOR HIGHER SEA TESTS

Also, for tests with a higher SEA (for both penetrating and nonpenetrating cases), there was significant tearing at the pegs, up to 4.445 cm (1.75-in.) for the small impactors and up to 13.97 cm (5.5-in.) for the larger impactors. Since each test had eight pegged locations, the total length of fabric tearing (or alternatively, the total number of torn yarns) at these pegs far exceeded the length of tearing (or the total number of torn yarns) at the impact region for the higher SEA tests. Previous quasistatic tests also demonstrated that a significant amount of energy can be absorbed by fabric tearing at pegs [5].

2.3 SUMMARY OF THE BALLISTIC TESTS.

Woven Zylon, when attached to a frame by pegs, has shown itself to be a very effective material for ballistic protection against fragment penetration, reaching SEAs of nearly 140 kJ/g/cm^2 (50 kft-lb/lb/ft^2). A large database of repeatable results was obtained during this program, and the key findings are summarized below, followed by a discussion of the questions raised by these experiments, and suggestions for future work to address these questions.

2.3.1 Key Findings.

The following list summarizes key results of the ballistic impact tests:

1. There was excellent experimental repeatability—SEA results for almost all repeat tests fell within the limits of measurement accuracy.

2. The fabric deflections were quite large, especially for tests where impactor did not penetrate (up to 27.9 cm (11 in.) for the small impactors; up to 48.3 cm (19 in.) for the large impactors).

3. Tearing of the fabric from one or more of the side pegs led to much higher SEAs.

4. The SEAs for the heavy Zylon and the baseline Zylon were the same; the SEA for Kevlar was 37% lower and for environmentally exposed Zylon 48% lower.

5. The 0.229-cm- (0.090-in.)-thick aluminum backing sheet had little effect on the SEA for Configuration A, but the 0.127-cm- (0.050-in.)-thick aluminum backing sheet with the field bolts in Configuration B significantly reduced the SEA.

6. For full-penetration, center impact, ≈45° roll tests

   - SEAs for Configuration A were nearly constant (slightly rising near ballistic limit) and approximately proportional to the area of the impact end of the impactor. (Note that large impactor is two times larger than small impactor for all dimensions.)

   - SEAs for Configuration B (without the aluminum backing sheet) were higher (≈30% for the large impactors, 0%-10% for the small impactors).

7. For off-center impact, ≈45° roll tests, the SEA was reduced (compared to center impact tests)

   - slightly (10%-20%) for the small impactors for Configuration A with the impact point centered 3.2 in. from the nearest peg.

   - negligibly for the small impactors for Configuration B 16.5 cm (6.5 in.) from the nearest peg.

   - by 20%-23% for the large impactors for Configuration B 16.5-23.4 cm (6.5-9.2 in.) from the nearest peg.

8. Roll angle (for Configuration A, center impact tests without the aluminum backing sheet) had a large effect on SEA; however, the effect was different for the two impactors.

   - For the large impactors, the SEAs of ≈0° roll tests were reduced (to only about 40% for ≈45° roll tests).

- For the small impactors, the SEAs of either ≈0° or ≈90° roll tests were increased (by ≥ 30%).

2.3.2 Questions and Issues.

The following is a list of questions or issues raised by the ballistic impact test results.

1. The aluminum backing sheet with the ≈0.476-cm- (≈3/16-in.)-diameter field bolts significantly reduced the SEA in Configuration B tests. Would weaker or no field bolts have eliminated this deleterious effect?

2. For the large impactor (Configuration A without the aluminum backing sheet, center impact), ≈0° roll angle tests resulted in SEAs ≈60% lower than those for ≈45° roll tests. Why is the difference so much greater than the 30% difference in the number of yarns directly impacted? Are the fabric failure modes different? Is proximity to the horizontal frame member a factor? Would 90° roll Configuration A tests or 0° roll Configuration B tests show less of a difference (in both of these, the impactor edges would be farther from any frame member)?

3. For the small impactor (Configuration A, center impact), ≈0° and ≈90°roll tests (with ≈0° yaw and pitch) had much higher SEAs than ≈45° roll tests (with ≈0° yaw and pitch). What is the cause of this counter-intuitive result? At 45° roll, do the impactor corners tear through fabric more easily?

4. A difference in SEA was seen for two tests (small impactor, ≈90° roll, center impact) that were identical except that the warp and fill directions of the fabric were reversed. Are these differences repeatable for other test conditions? If so, would a better barrier design include a 90° rotation of the fabric orientation for alternate plies?

5. Tearing of the fabric at the side pegs increased the SEA. Would a better barrier design have the side pegs closer to the fabric edge, to encourage fabric tear off?

6. For the large impactors, the shortest distance from the off-center impact location midpoint to the closest peg was 16.5 cm (6.5 in.), which resulted in SEAs ≤23% less than the center impact tests. How much larger a reduction in SEA would result from impacts even closer to the side pegs?

7. The heavy Zylon (1500-Denier, 17x17 fabric) significantly outperformed the baseline Zylon (500-Denier, 35x35 fabric) in National Aeronautics and Space Administration's (NASA) ballistic ring tests, but the two fabrics behaved the same in SRI's pegged barrier tests. What is it about the different attachment geometries that lead to these different results?

2.3.3 Suggested Future Work.

The answers to most of the issues raised in the previous section can be obtained by one additional series of full-scale ballistic impact tests, using the existing frames for Configurations A and B. Such a series could include the following tests with the baseline Zy35 fabric.

1. Configuration B tests (center impact, 45° roll) with the aluminum backing sheet, but without any field bolts—to answer question 1 above—followed perhaps by some tests with thinner or weaker field bolts than those used in this program.

2. Large impactor Configuration A (center impact, with no backing sheet), tests with 90° roll and Configuration B tests with 0° (and 90°) roll—to answer question 2 above.

3. Small impactor (Configuration A, center impact, with no backing sheet) tests with 0° and 90° roll at higher velocities (farther away from the ballistic limit) than those reached thus far—to answer question 3 above.

4. Large impactor tests (Configurations A or B, with no backing sheet) at 0° or 90° roll, varying the orientation of the fill and warp yarns—to answer question 4 above.

5. Large impactor (Configuration B, with no backing sheet, 45° roll) tests, repeating higher SEA tests (e.g., tests 41 or 52) in which the impactor penetrated and the fabric had large amounts of tearing at the pegs, but did not tear off. In these proposed tests, the distance from the pegged holes to the fabric edge would be reduced to the point where the fabric was likely to tear off—to answer question 5 above.

6. Large impactor (Configuration A, with no backing sheet, 45° roll) tests with the impact location as close to a side peg as possible—to answer question 6 above.

In addition, with a slight modification to an existing frame used in an earlier test series at Naval Air Warfare Center, China Lake [5], that allows continuous wrapping of fabric around two rods, impact tests could be performed on the baseline Zylon and the heavy Zylon to address the issue (raised in question 7) of these two materials behaving the same in pegged tests but differently in wrapped tests.

3. METHODS FOR CUTTING HOLES IN ZYLON FABRIC.

Cutting holes in the Zylon (or other high-strength) fabric has been an issue in performing the ballistic impact tests in this and previous programs, which used pegging through the fabric as a means of attachment. If the use of Zylon in aircraft is to become commercially viable, a time- and cost-effective method for cutting holes in multiple layers of fabric plies needs to be found.

3.1 PREVIOUS METHODS.

In previous programs, several methods have been used for making the holes (which ranged from 0.635 to 2.54 cm (0.25 to 1.0 in.) in diameter). Holes have been cut out with ceramic scissors or finely serrated metallic scissors. Holes have also been cut with a ceramic knife, with the fabric positioned on a hard surface. Both methods were tedious and worked only on a few plies at a time (only one ply at a time with the scissors).

3.2 CURRENT METHODS.

For this program, a variety of methods were tried for cutting holes in multiple plies. These included punching holes with a circular punch, drilling holes with a circular core drill, and using an awl to create and then enlarge holes without cutting any yarns. The first two were unsatisfactory—sometimes they worked, but only with a significant amount of force and only on one ply at a time. The awl method worked fine for holes up to about 0.476 cm (3/16 in.) but no larger.

The method that was used for this program's tests was slicing through the fabric with a commercially available two-edged, high-carbon steel arrowhead.* (A commercial four-edged arrowhead could not be found, and an attempt to machine such a tool was not successful.) The arrowhead, attached to an aluminum grip, was thrust through a hole in an aluminum template into as many as six (but usually only four) plies of the fabric at two perpendicular directions, piercing a hole in the fabric sufficient to allow the insertion of the 1.27-cm- (1/2-in.)-diameter bolt. During the process, force was exerted on the fabric by pressing one's weight on the aluminum template to minimize any movement of the fabric during the piercing. The first thrust usually went through easily, but the second perpendicular thrust did not cut as many yarns as was required without sawing the blade back and forth a few times.

Although this technique worked fairly well for four plies at a time, it was tiring, and after a few holes, the arrowhead began to dull and needed replacement or sharpening. It became clear that a better method was needed to produce many holes in multiple layers.

3.3 RECOMMENDED FUTURE METHOD—LASER CUTTING.

A commercial laser-cutting company was contacted, and they used a carbon dioxide (CO_2) laser to cut holes in the Zylon fabric. The fabric was clamped onto a large moving table and the laser

---

* The arrowhead was a Two-Edged 11/32 Black Diamond Broadhead, manufactured by Zwickey Archery Inc. of St. Paul, MN.

was used, not in a continuous mode, but instead was pulsed on and off rapidly as the table with the fabric moved under it in a computer-controlled path.

The laser parameters were 2.5-psi CO_2 gas pressure, 550-watt laser power, 250-Hz pulse frequency, 65% duty cycle (percentage of time laser was on), and 20-in./min. feed rate. These are not necessarily the optimal parameters, but were the first set of parameters tried. With them, a 2.54-cm- (1-in.)-diameter hole was cut into 48 plies of Zylon in one pass. The edges of the cut were charred for a distance of less than 0.127 cm (0.05 in.) (as shown in figure 3-1), but no damage to the fabric was apparent beyond that distance. Unraveling of the yarns or individual fibers appeared to be inhibited by the charring, which was much less than with any other of the techniques described. An attempt at cutting 96 plies with the same parameters was almost successful—only the last few plies did not cut all of the way around on the first pass. A slight change in the laser parameters would likely allow successful cutting of 96 or more plies.

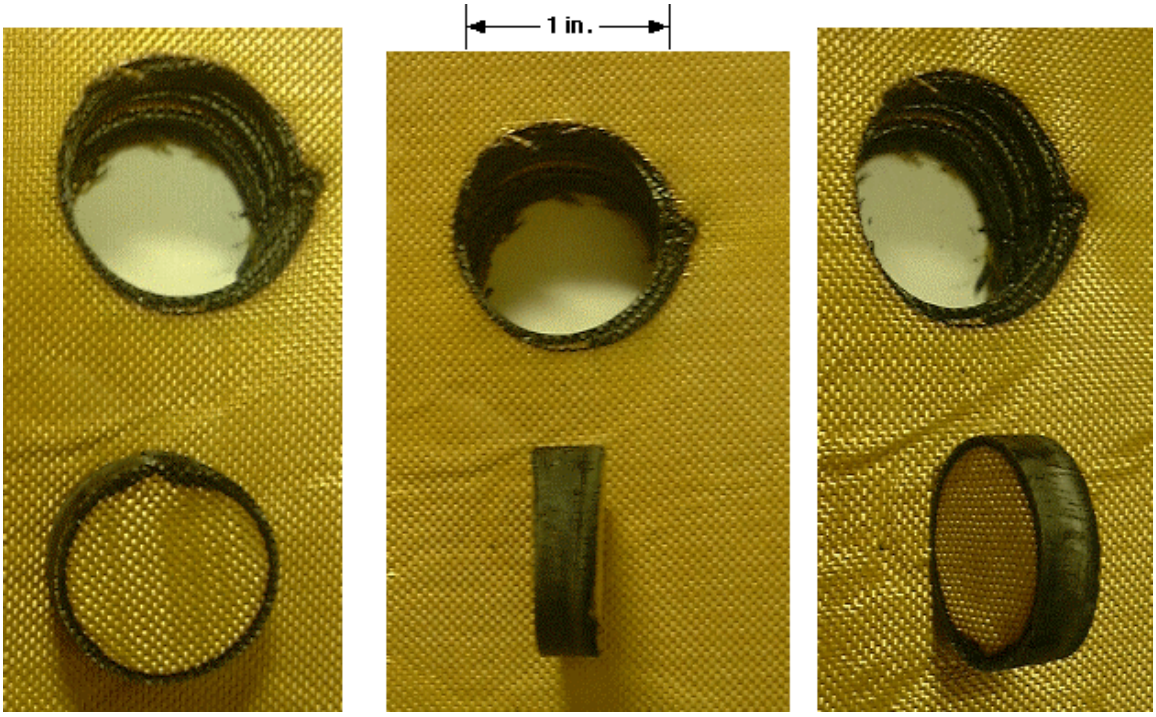

FIGURE 3-1. THREE VIEWS OF A 2.54-cm- (1-in.)-DIAMETER HOLE LASER-CUT INTO 48 PLIES OF Zy35 FABRIC

The cost at this particular commercial laser-cutting operation was $350/min. for laser time plus $150/hour for a 1-time programming setup. Computer-aided design programs can be used to control the laser table motion, so holes for the pegs and the exterior shape of the fabric barrier could be cut during one operation, if desired. Since many holes can be cut in many layers of fabric in a short time, laser cutting appears to be a cost-effective method to produce ballistic barriers attachable to airframes.

4. FINITE ELEMENT ANALYSIS.

A computational model is being developed that can be used as a design tool for choosing or evaluating parameters for fragment barriers containing ballistic fabric. The design model, implemented into the LS-DYNA3D finite element code, uses shell elements with an orthotropic continuum formulation to model the fabric. Because calculations run relatively quickly (about 2 hours using a four-processor Pentium III Linux cluster for an 80,000 element simulation of a gas-gun experiment), the model allows evaluation of variations in design parameters such as size of fabric; gripping conditions; number of fabric plies or yarn pitch; and size, orientation, and velocity of a fragment. The goal is to use the model to design and verify fragment barriers; for example, to determine how many plies of woven fabric are needed to stop a given fragment threat and to compute the loads applied to the supporting structure.

In this investigation, simulations were performed on the large-scale ballistic impact tests described above. A total of 15 simulations were performed, investigating the effects of the different frame configurations; number of fabric plies; and the size, velocity, and orientation of the impactor. Only tests with no aluminum backing and using the standard Zylon fabric were simulated. The calculations were run using LS-DYNA3D version 970 beta revision 2825.

4.1 FINITE ELEMENT MODEL.

As shown in figure 4-1, finite element models were developed for the two target configurations, A and B. The box beams comprising the frames were modeled using shell elements. In the model, the box beams had dimensions of 7.6 by 5.1 cm (3.0 by 2.0 in.), a wall thickness of 0.63 cm (0.25 in.), and rounded edges with a radius of curvature of approximately 1.3 cm (0.5 in.). Attachment of the fabric to the frame was the same as in the experiment. Square holes were made in the fabric and positioned over 1.27-cm- (1/2 in.)-diameter steel bolts. The fabric extended 12.7 cm (5 inches) beyond the edges to allow tearing to occur.

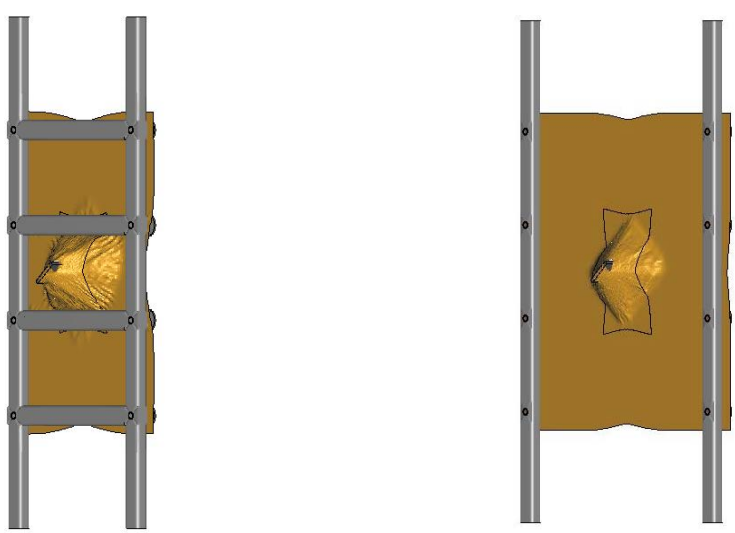

(a) Configuration A (b) Configuration B

FIGURE 4-1. FINITE ELEMENT MODEL OF FRAME CONFIGURATIONS

The model for Configuration A, shown in figure 4-1(a), has four horizontal beams, centered 32.3 cm (12.7 in.) apart, rigidly attached between two vertical beams, centered 61 cm (24 in.) apart. The end sections of the vertical beams above and below the fabric were modeled as fixed. The model for Configuration B, shown in figure 4-1(b) consists of two vertical beams centered 96.5 cm (38 in.) apart, with four 1.27-cm (1/2-in.-diameter pegs spaced 32.3 cm (12.7 in.) apart.

For most of the tests, the impact location was at the center of the target, midway between the two vertical beams. For three of the simulations, the impact location was off-center, as close as feasible to one beam (16.5 or 23.4 cm (6.5 or 9.2 in.) from the center of the nearest peg).

Two impactors were modeled, as shown in figure 4-2. The smaller impactor was a 5.08- by 5.08- by 0.63-cm (2.0- by 2.0- by 0.25-in.)-rectangular plate that weighed 128 g (0.28 lb), and the larger impactor was a 10.16- by 10.16- by 1.27-cm (4.0- by 4.0- by 0.50-in.)-rectangular plate that weighed 1022 g (2.25 lb). The large impactor model weighed about 3% more than measured in the experiment.

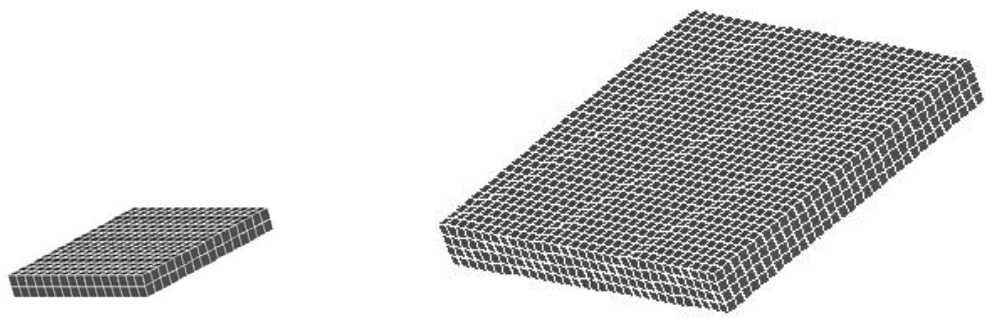

(a) Small impactor (b) Large impactor

FIGURE 4-2. IMPACTOR MODEL

4.2 FINITE ELEMENT MESH.

The finite element mesh used 0.635-cm (1/4-in.) elements for most of the fabric. To better capture the stress gradients leading to damage, a finer mesh resolution was used around the pegs 0.318 cm (1/8 in.) and at the impact location. In 20.32-cm (8-in.) square around the impact location, four fabric elements were used across the smallest dimension of the impactor, i.e., for the large impactor a mesh resolution of 0.318 cm (1/8 in.) was used and for the small impactor a mesh resolution of 0.159 cm (1/16 in.) was used. The mesh resolution for the impactors, shown in figure 4-2, was 0.318 cm (1/8 in.).

In every case, the fabric was modeled with a single layer of shell elements. To account for the two target thicknesses, 4 layers and 12 layers, the thickness of the shell elements was varied. Note that because the fabric is modeled as a continuum, the element thickness is only about 1/4 of the measured thickness of the fabric.

The total number of elements in the model varied from 52,560 for Configuration A with a small impactor to 66,144 for Configuration B with a large impactor. The Belytschko-Tsay [6] shell

element formulation was used, but to minimize bending stiffness, single-point integration through the thickness was used.

4.3 MATERIAL MODELS.

The steel specified for the frame was A500C carbon steel, which, according to the manufacturer's specifications, has a minimum yield strength of 345 MPa (50 ksi), a minimum ultimate strength of 428 MPa (62 ksi), and a minimum elongation to failure of 21%. The steel for the impactor and frame was modeled as elastic with a Young's modulus of 30×10^6 psi, a Poisson's ratio of 0.3, and a density of 7.8 g/cc.

Only tests with the baseline Zylon were analyzed. The SRI ballistic fabric model was used, with parameters chosen for Zylon based on quasi-static tests performed at Arizona State University and SRI and impact tests performed at NASA Glenn. The model is implemented in LS-DYNA as a user-defined material model [7]. Constants for Zylon are given in table 4-1. Slack in the fabric was approximated by including an additional 10% strain in the fabric crimp, i.e., the actual fabric crimp in the x direction is 0.037, but a value of 0.137 was entered to account for fabric slack.

TABLE 4-1. CONSTANTS FOR ZYLON

Name	Symbol	Value
Tensile Modulus	E	13.3Msi
Peak stress	σ_{max}	0.42 Msi
Initial damage strain	ε_{min}	0.025
Strain at peak stress	ε_{max}	0.036
Crimp strain x direction	ε_{crx}	0.137
Crimp strain y direction	ε_{cry}	0.106
Failure strain	ε_f	0.01
Crimp modulus	E_{cr}	0.047
Compression modulus	E_{co}	0.005
Time constant	τ	3.0 μs
Density	ρ	2.88 g/cm3
Shell thickness	t	0.0031 in/ply

In a region extending from 5.1 cm (2 in.) inside the attachments to the edge of the fabric and 7.6 cm (3 in.) above and below the attachments, the strength of the fabric was arbitrarily reduced by half to facilitate tearing in the fabric. Tearing of the fabric at the attachments has a large effect on the energy absorbed by the fabric, and the standard parameters chosen to match failure at the impactor resulted in too little tearing at the attachments. If the fabric at the attachments is too strong to tear, the impactor breaks through the fabric at the impact location too soon, resulting in too little energy absorbed.

4.4 SLIDELINE TREATMENT.

In developing the material model, it was shown that the choice of slideline formulation and slideline parameters can make a large difference in the results [6]. For these analyses, the slideline formulation chosen was AUTOMATIC_SURFACE_TO_SURFACE slideline with segment checks on interpenetration (set parameter soft=2). All other slideline parameters were set to default values.

4.5 MODEL RESULTS.

The results of the simulations are listed in table 4-2, which gives calculated values for residual velocity of the impactor and energy absorbed by the fabric, as well the ratio of the calculated energy absorbed to the measured energy absorbed. Overall, the agreement between the model and experiments is quite good. As shown in table 4-3, the average value of the ratio of the energy absorbed in the model simulation to the experimental value is 0.98 with a standard deviation of 0.25.

TABLE 4-2. RESULTS OF MODEL SIMULATIONS FOR CHES TESTS

Test	Configur-ation	Impactor						Fabric Target				Comments
		Mass (g)	Roll (deg)	Impact Velocity (m/s)	Residual Velocity		Kinetic Energy ($kJ/g/cm^2$)	No. Plies	Absorbed Energy			
					Experiment (m/s)	Model (m/s)			Experiment ($kJ/g/cm^2$)	Model ($kJ/g/cm^2$)	Ratio	
1	A						21.4	4				
62	A				0	138	37.1	4	37.1	17.7	0.48	
10	A	128	47	192	141	119	37.4	4	17.3	23.1	1.34	
58	A	128	54	192	148	148	37.4	4	15.2	15.2	1.00	Off-center
60	A	128	90	196	0	106	39.0	4	39.0	27.6	0.71	
3	A	128	57	225	182	177	51.4	4	17.8	19.6	1.10	
14	A	990	43	150	118	123	177	4	67.4	57.9	0.86	
13	A	990	51	188	0	95	92.6	12	92.6	68.9	0.74	
27	A	990	10	209	173	165	114	12	36.0	43.1	1.20	
21	A	990	45	211	105	130	117	12	87.7	72.3	0.82	
17	A	990	48	229	151	152	137	12	77.6	76.8	0.99	
56	B	128	48	232	184	168	55	4	20.3	26.0	1.28	Off-center
51	B	128	56	246	214	198	61.5	4	15.0	21.7	1.45	
41	B	990	49	226	104	136	134	12	105	85.3	0.81	
52	B	990	49	230	143	152	139	12	85.0	78.0	0.92	Off-center

TABLE 4-3. RATIO OF MODEL TO EXPERIMENT ENERGY ABSORBED

Configuration	Impactor	Average	Standard Deviation
All	All	0.98	0.25
A	Small	0.94	0.28
A	Large	0.92	0.16
B	Small	1.36	0.08
B	Large	0.86	0.05

For Configuration A, the largest discrepancies are found for tests where the impactor did not penetrate, but the simulation predicted penetration (tests 62, 60, and 13), in which case the model significantly underpredicted the energy absorbed. This may be due to effects of impactor orientation that were not included in the analysis, i.e., impactor pitch and yaw that caused the impactor to tumble and thus not penetrate. For Configuration B, the model consistently underpredicted the energy absorbed for the large impactor, probably because the model had significantly less tearing than in the tests, and overpredicted the energy absorbed for the small impactor. The results of the simulations are reviewed in groups by configuration and impactor size, then variations due to configuration, impact location, and roll angle are discussed below.

Figure 4-3 shows the results of simulations of Configuration A tests and the small impactor in terms of energy absorbed per areal density of fabric as a function of impact energy per areal density of fabric. For these six tests, the average ratio of the energy absorbed in the simulations to that of the experiment was 0.94 with a standard deviation of 0.28. For the tests with center impact and nominal 45º roll, the model gave very close predictions for two of the tests (01 and 03) but overpredicted the energy absorbed for one test (test 10). The model exactly matched the energy absorbed for the one off-center test (test 58) and significantly underpredicted the energy absorbed for the tests with nominal 0º and 90º roll angles (tests 60 and 62).

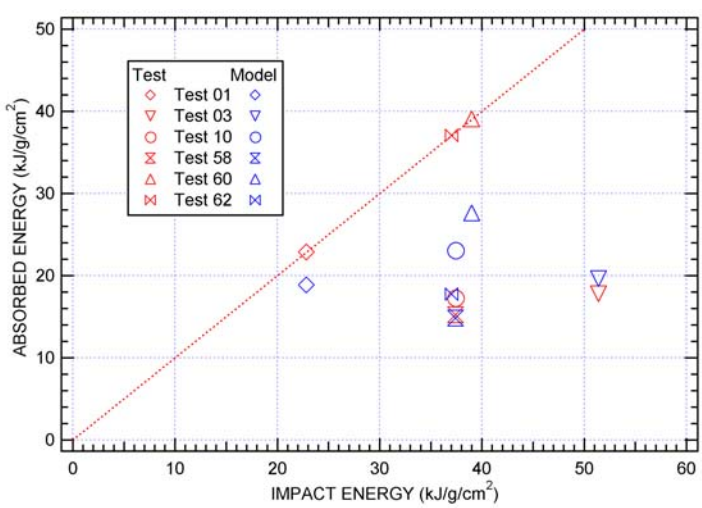

FIGURE 4-3. SIMULATIONS OF CONFIGURATION A TESTS WITH THE SMALL IMPACTOR

Figure 4-4 shows the results of simulations of Configuration A tests and the large impactor. For these five tests, the average ratio of the energy absorbed in the simulations to that of the experiment was 0.92 with a standard deviation of 0.16. For three of the tests with center impact and nominal 45º roll (tests 14, 17, and 21), the model gave consistently close (but slightly under) predictions for energy absorbed. For the fourth test (test 13), the model underpredicted the energy absorbed by 26%. The model overpredicted the energy absorbed for the test with nominal 0º roll angle (test 27).

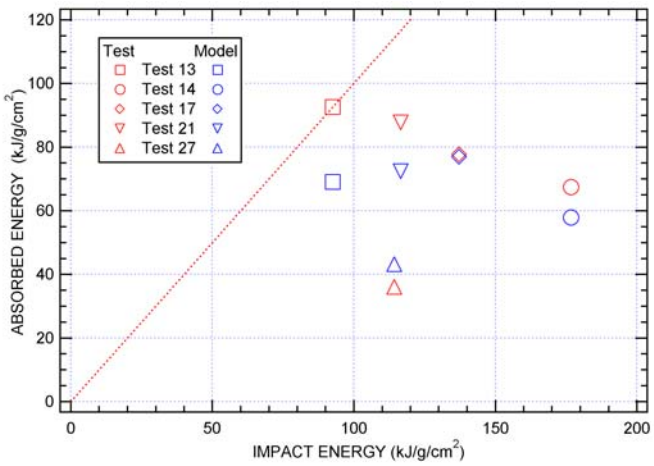

FIGURE 4-4. SIMULATION OF CONFIGURATION A, LARGE IMPACTOR

Figure 4-5 shows the results of the four simulations of Configuration B tests. The model overpredicted the energy absorbed for the two tests with the small impactor (tests 51 and 56). For these two tests, the ratio of the simulated to measured energy absorbed was 1.36 and the standard deviation was 0.08. The model underpredicted the energy absorbed for the two tests with the small impactor (tests 41 and 52). For these two tests, the ratio of the simulated to measured energy absorbed was 0.86 and the standard deviation was 0.05.

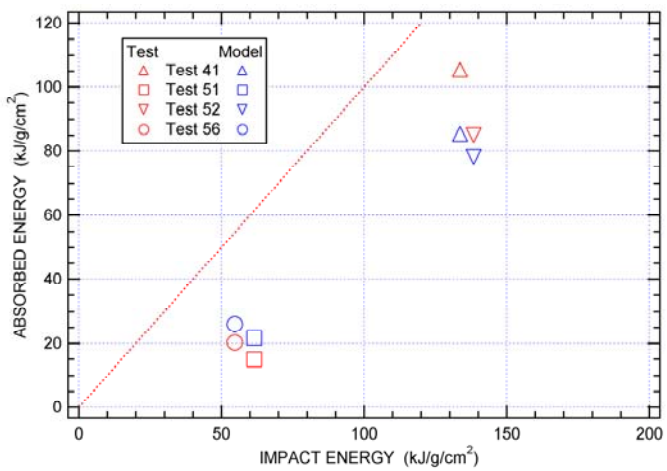

FIGURE 4-5. SIMULATION OF CONFIGURATION B TESTS

Figure 4-6 shows the results of the simulations comparing Configuration A (tests 03 and 17) with Configuration B (tests 41 and 51). For the small impactor, the model predicted no significant difference in energy absorbed between Configurations A and B, which was consistent with the experimental findings. For the large impactor, the model predicted more energy absorbed for Configuration B than A, but the effect was less than observed in the experiments.

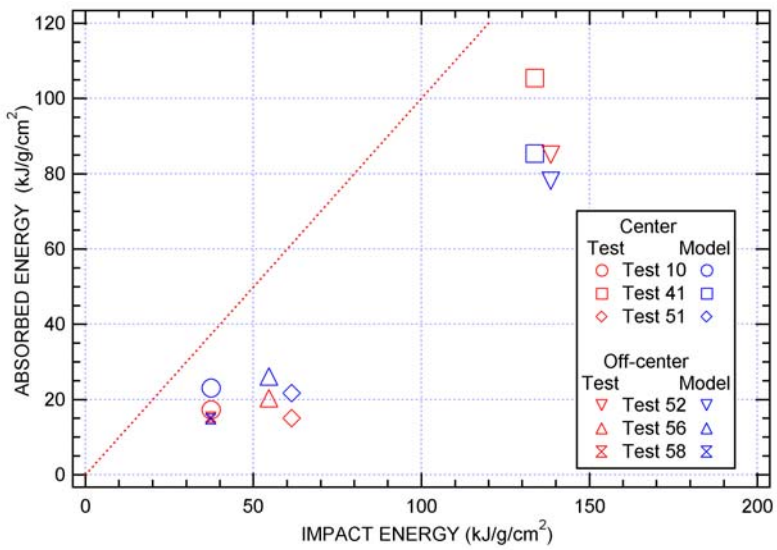

FIGURE 4-6. SIMULATIONS OF CONFIGURATION A VS B

Figure 4-7 shows the results of the simulations investigating the effect of off-center impacts. For the small impactor, the model predictions were consistent with the experimental findings. For the large impactor, the model predicted less energy absorbed for the off-center impact, but the effect was less than observed in the experiments.

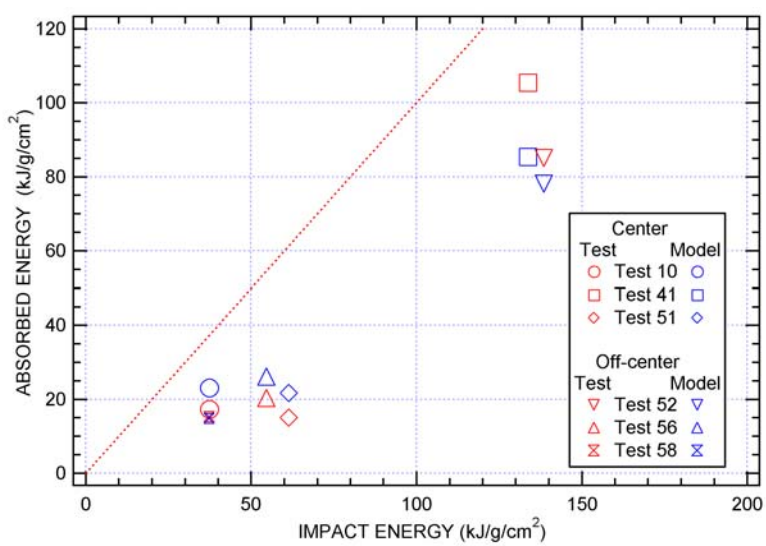

FIGURE 4-7. SIMULATION OF OFF-CENTER TESTS

Figure 4-8 shows the results of the simulations investigating roll angle. For the small impactor, the model predicted slightly higher energy absorbed for the 11º and 90º tests compared to the 47º test. In the tests, the 47º impactor penetrated the fabric, but the 11º and 90º impactors were stopped, resulting in a large difference in energy absorbed. For the large impactor, the model predicted less energy absorbed for the 10º roll test compared to the 45º test, which was consistent with the experimental results, but the effect was greater in the experiments.

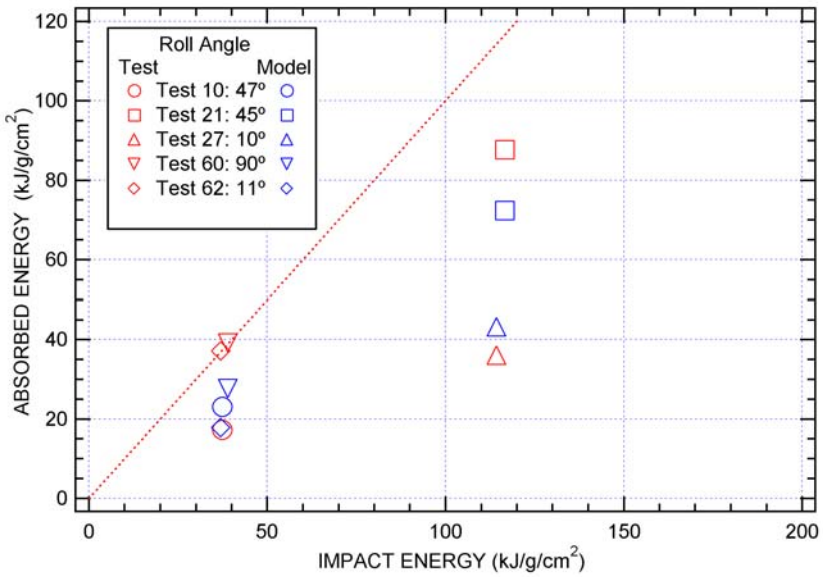

FIGURE 4-8. SIMULATIONS OF ROLL ANGLE

4.6 FABRIC DEFORMATION AND FAILURE.

Representative responses of fabric deformation and failure from several tests are discussed below. Still photographs were taken from the high-speed video and compared with the calculated response at an equivalent time after impact. In general, the model showed good overall agreement in the deformed shape of the fabric during impact; however, the experiments showed greater fabric deformation than the model for both tests in which the impactor penetrated the fabric and in tests where the penetrator was contained. This difference was likely due to slack in the fabric that was not modeled correctly.

4.6.1 Test 1.

Figure 4-9 shows the measured and calculated deformation of the fabric for test 1, the small fragment with an impact velocity of 150 m/s (492 ft/s). The fragment was stopped both in the experiment and the simulation. At 0.9 ms after impact, the shape of the displaced fabric in the model was very close to that in the experiment. However, by 1.9 ms, the displacement in the simulation is near the peak value of 16.5 cm (6.5 in.), while the fabric in the experiment continues to deform to a maximum displacement of 21.6 cm (8.5 in.). The likely explanation for this difference was that in the experiment, the fabric had slack that was not included in the model.

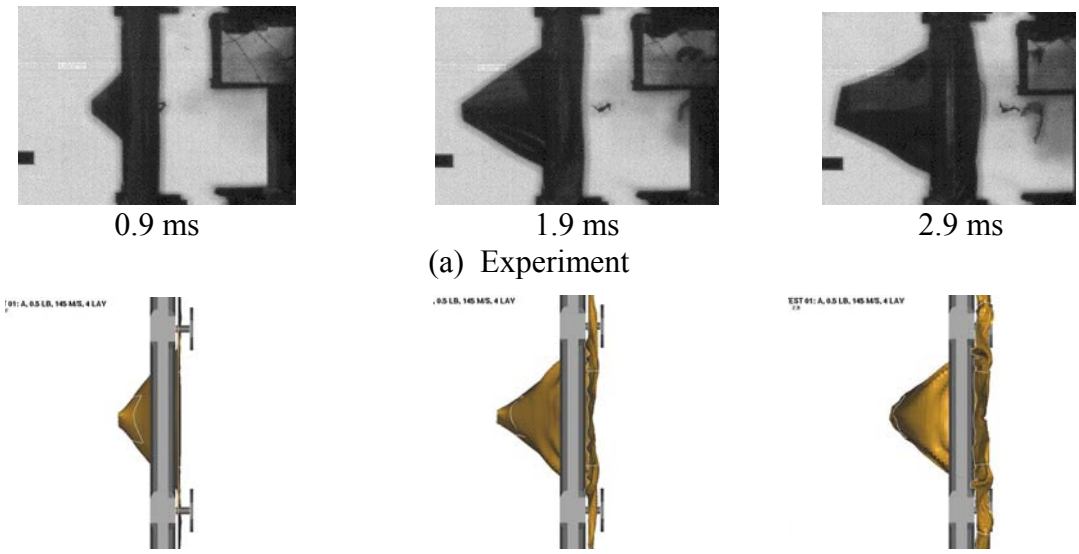

FIGURE 4-9. FABRIC DEFORMATION FOR TEST 01

4.6.2 Test 3.

Figure 4-10 shows the measured and calculated deformation of the fabric for test 3, the small fragment with an impact velocity of 225 m/s (738 ft/s). The residual velocity in the experiment was 182 m/s (597 ft/s) and 177 m/s (581 ft/s) in the simulation; that is, the model absorbed about 10% more energy than in the experiment. Similar to the response of test 1, there was greater deformation in the fabric in the experiment than in the simulation; the fragment appeared to penetrate the fabric sooner in the model. Again, the likely explanation for this difference is slack in the fabric, which was not accurately included in the model.

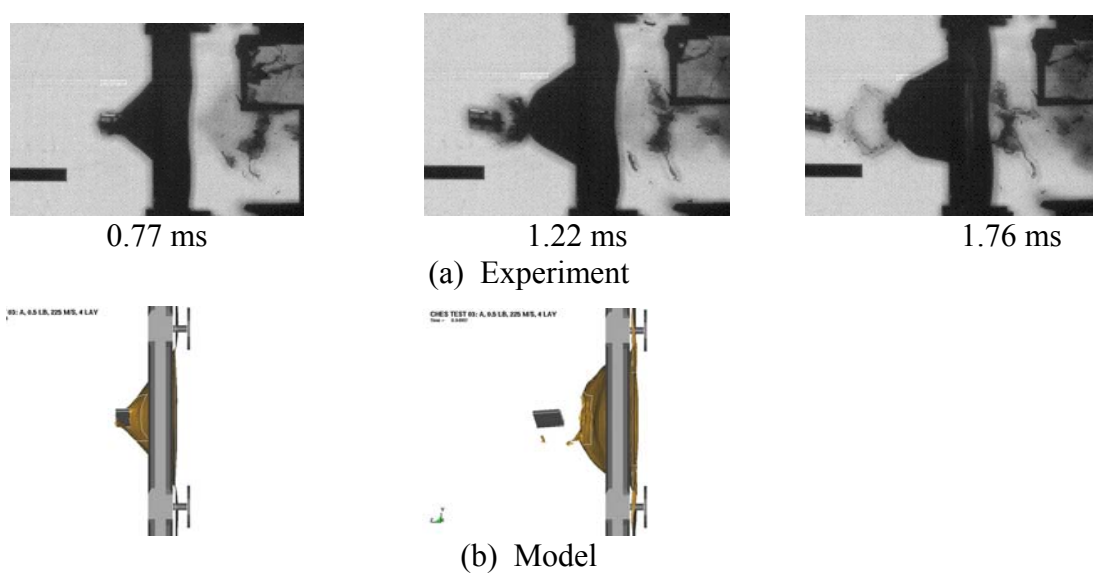

FIGURE 4-10. FABRIC DEFORMATION FOR TEST 03

4.6.3 Test 17.

Figure 4-11 shows the measured and calculated deformation of the fabric for test 17, the large impactor with an impact velocity of 229 m/s (751 ft/s). The residual velocity in the simulation experiment was 152 m/s (499 ft/s)—almost exactly as in the experiment (151 m/s) (495 ft/s). At 1.27 ms, the impactor penetrated some of the fabric in the experiment (i.e., the corners are clearly sticking though the fabric), but in the simulation, more of the penetrator was showing. Again, the slack in the fabric may be the cause of this discrepancy, but also the fact that the fabric is actually 12 separate plies that all need to be penetrated before the impactor is through. In the model, the fabric is modeled by a single layer of shell elements that are either failed or not.

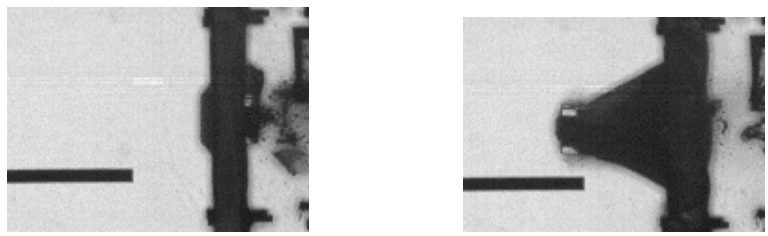

0.37 ms 1.27 ms

(a) Experiment

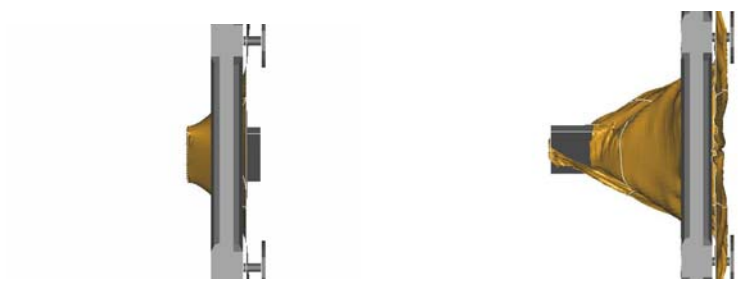

(b) Model

FIGURE 4-11. FABRIC DEFORMATION FOR TEST 10

4.7 FABRIC FAILURE MECHANISM.

The failure mechanism for the fabric at the impactor is tearing in a rectangular pattern, even if the impactor is at a 45°angle to the yarn orientation, as shown in figure 4-12(a) for test 21, which had the large impactor at 211 m/s (692 ft/s) in Configuration A. This failure mechanism was captured in the simulations as well, as shown in figure 4-12(b), which shows the failed elements around the impactor as a basically horizontal tear connecting two vertical tears. A similar failure mechanism is shown in figure 4-12(c) for the small impactor in test 10.

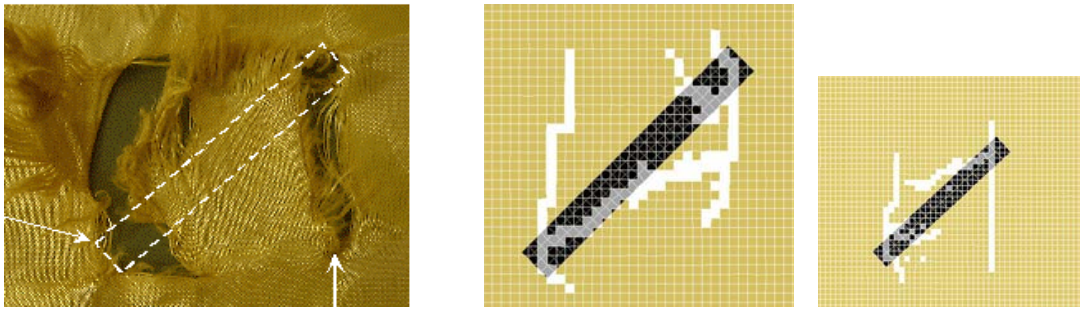

(a) Test 21 Experiment (b) Test 21 Model (c) Test 10 Model

FIGURE 4-12. FABRIC TEARING AT THE IMPACTOR

The mechanism of fabric failure at the attachment pegs is a tearing away at the peg in a line from the peg towards the impactor, as shown in figure 4-13(a) for test 21. In the simulation, shown in figure 4-13(b), some tearing at the attachment occurred, but less than what occurred in the experiment and the line of tearing is off-line from the impactor. Figure 4-13(c) shows the calculated tearing for test 41, which had more tearing than test 21, and the mechanism of tearing, in a line away from the attachment towards the impactor is clearly correct.

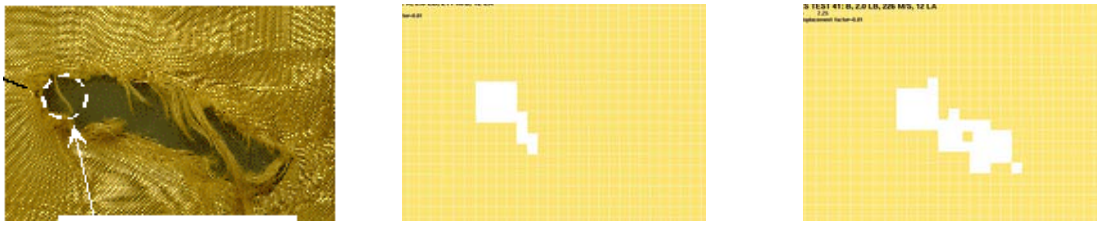

(a) Test 21 Experiment (b) Test 21 Model (c) Test 41 Model

FIGURE 4-13. FABRIC TEARING AT THE ATTACHMENT

5. SUMMARY AND RECOMMENDATIONS.

5.1 SUMMARY.

A total of 63 experiments were performed, 54 of which produced unequivocal data. Repeatability of results was excellent. Zylon® fabric was highly efficient in absorbing projectile energy, absorbing nearly 140 kJ/g/cm^2 (50 kft-lb/lb/ft^2) or about 50% more than Kevlar® at equivalent weight. Exposure of Zylon fabric to high humidity at 160°F for 3 weeks decreased the energy absorbed by 48%.

It was found that tearing of the fabric where it was attached to the frame absorbed considerable energy, suggesting that attachment could be designed to maximize barrier effectiveness.

An unattached aluminum backing sheet had little effect on absorbed energy, but a sheet attached to the Zylon blanket with field bolts reduced the absorbed energy considerably.

Off-center impacts reduced the absorbed energy for certain frame configurations and projectile sizes by as much as 23%.

Simulations of experiments using the LS-DYNA3D finite element code and the Federal Aviation Administration-funded SRI International fabric model showed good agreement with measurements. The average ratio of calculated energy absorbed to measured energy absorbed was 0.98 with a standard deviation of 0.25. The model correctly predicted the fabric damage mechanism—tearing in a rectangular pattern at the impact site, and tearing in a line away from attachments toward the impact site. However, computed deformation was significantly less than measured, probably because slack in the fabric was not modeled.

The experiments and computations reported here suggest that lightweight barriers of ballistic fabric are practical solutions to uncontained engine debris protection. However, a number of issues are not understood at this time. The actions needed to resolve these issues are listed in the following paragraphs.

Simulations were performed for 15 of the large-scale ballistic impact tests over a wide range of testing conditions, including both frame configurations, large and small impactors, 4 and 12 layers of fabric, center and off-center impact locations, and a range of impactor velocity and roll angle. Overall, the model shows good agreement with the test results. The average ratio of calculated energy absorbed to measured energy absorbed was 0.98 with a standard deviation of 0.25. The model gets the damage mechanism correct, tearing in a rectangular pattern at the impactor, and tearing in a line away from attachment points oriented towards the impactor.

The model does a fairly good job in representing the fabric deformation, but the deformation in the simulations are considerably less than in the tests, probably because the slack in the fabric is not accurately represented in the model.

It is understood that these simulations are very difficult to get right because the analyses are quite sensitive to many factors both physical and numerical in addition to the material model, including such things as solution parameters, particularly slideline parameters, element formulation, mesh resolution, attachment details, and impactor orientation.

Some of the test results are not yet understood and more analysis is needed. For example, the effect of roll angle is not consistent for the small and large impactor. For the large impactor, a roll angle of 0° results in less energy absorbed than for 45°. This is expected because fewer yarns are cut. However, for the small impactor, orienting the impactor with a roll angle of 0° or 90° results in considerably more energy absorbed than for 45°. This may be due to effects of pitch and yaw in the impactor, i.e., at 0° and 90°, the impactor is easier to tumble.

The energy absorbed is a balance between ripping at impactor and tearing at attachments. If the fabric is too strong at the attachments, the impactor penetrates the barrier and absorbs significantly less energy. In the simulations, the model tore less at the attachments than measured in the experiments. This is probably a combination of more development needed in the model for tearing at the attachments and also better representing the slack in the fabric.

5.2 RECOMMENDATIONS.

1. Further investigation of the effects of impactor orientation, including pitch and yaw. For example, if the impactor hits with a corner first, it may penetrate more easily than if it hits simultaneously along its edge. Also, if an impactor hits at an angle, it may be easier to tumble and, hence, not penetrate the fabric.

2. Improve the tearing model at attachments. Although the model gets the mechanism of tearing correct at the attachments, the extent of the tearing in the simulations was considerably less than in the experiments, even though the strength of the material around the attachments was reduced to promote tearing. It is likely that other choices of solution parameters will provide a better simulation of tearing response at the attachments. Test results of corner pull tests should be used to help develop the model.

3. Sensitivity of the results to material constants. Material constants were taken from static uniaxial tests and ring tests performed at SRI and Arizona State University. A dynamic time constant was added to improve the results for dynamic ring tests at the National Aeronautics and Space Administration. To generalize the model, it is important to realize which of the material constants significantly affect the response. Thus, when new materials are modeled, only the parameters found to be important need to be measured.

4. Mesh sensitivity. In the simulations, mesh density was chosen to be four elements across the smallest dimension of the impactor, which gave consistent results for large and small impactors. No comprehensive study was performed to demonstrate mesh sensitivity, although early simulations that used uniform 0.635-cm (1/4-in.) elements gave results that showed the fabric model was much too strong for small impactors.

5. Fabric crimp. Fabric crimp was included in the model because it is a fabric property that is relatively easy to measure. But slack, which depends on how the fabric is attached, was not accurately included. Both crimp and slack can be modeled by the same phenomenon, namely, deformation with very little stress generated, but slack is harder to quantify. It may be possible to quantify slack in these experiments by comparing computed and measured velocity histories, i.e., for fabric with more slack the impactor will decelerate more slowly.

6. REFERENCES.

1. Shockey, D.A., Simons, J.W., and Erlich, D.C., "Improved Barriers to Turbine Engine Fragments: Interim Report II," FAA report DOT/FAA/AR-99/8, II, May 1999.

2. "PBO Fiber Zylon," Technical Information, Toyobo Co., Ltd., Osaka, Japan, Rev. September 2001.

3. Shockey, D.A., Simons, J.W., and Erlich, D.C., "Improved Barriers to Turbine Engine Fragments: Interim Report I," FAA report DOT/FAA/AR-99/8,I, June 1999.

4. Shockey, D.A., Simons, J.W., and Erlich, D.C., "Improved Barriers to Turbine Engine Fragments: Interim Report III," FAA report DOT/FAA/AR-99/8,III, May 2001.

5. Shockey, D.A., Simons, J.W., and Erlich, D.C., "Improved Barriers to Turbine Engine Fragments: Interim Report V," FAA report DOT/FAA/AR-99/8,V, June 2002.

6. LS-DYNA User Manual, http:www.lstc.com.

7. Shockey, D.A., Simons, J.W., and Erlich, D.C., "Explicit Finite Element Analysis Modeling of Multi-Layer Composite Fabric for Gas Turbine Engines Containment Systems," summary report for ASU, Dept. of Civil and Environmental Engineering, March 2002.

APPENDIX A—PLAN FOR BALLISTIC TESTING OF ZYLON FABRIC

LIGHTWEIGHT BALLISTIC PROTECTION OF FLIGHT-CRITICAL COMPONENTS ON COMMERCIAL AIRCRAFT

PLAN FOR BALLISTIC TESTING OF ZYLON FABRIC

Written by: Jerry Farstad and Jennifer Zielinski
The Boeing Company
Seattle, WA 98124

TABLE OF CONTENTS

	Page
EXECUTIVE SUMMARY	v
A1. INTRODUCTION AND BACKGROUND.	1
A2. SMALL-SCALE LABORATORY TESTS OF ZYLON FABRIC BALLISTIC PERFORMANCE	2
A3. AIRPLANE SCALE TESTS OF ZYLON FABRIC BALLISTIC PERFORMANCE	7
A4. CONCLUSION	10

LIST OF FIGURES

Figure Page

FIGURE A1. Schematic for small scale laboratory test of Zylon fabric ballistic properties: bare fabric targets with clamped edge conditions.

FIGURE A2. Schematic for small-scale laboratory test of Zylon fabric ballistic properties: bare fabric targets with edges constrained by discrete fasteners.

FIGURE A3. Schematic for small-scale laboratory test of Zylon fabric ballistic properties: aluminum sheet and Zylon fabric targets with clamped edge conditions.

FIGURE A4. Schematic for small scale laboratory test of Zylon fabric ballistic properties: Multiple simultaneous projectiles with clamped edge conditions.

FIGURE A5. Schematic for airplane scale test of Zylon fabric ballistic properties: aluminum sheet and zylon fabric targets attached to ladder frame similar to commercial airplane fuselage structure.

FIGURE A6. Schematic for airplane scale test of Zylon fabric ballistic properties: aluminum sheet and zylon fabric targets attached to steel frame similar to commercial airplane fan cowl structure.

FIGURE A7. Schematic for airplane scale test of Zylon fabric ballistic properties: Zylon fabric shield installed of salvaged transport airplane fuselage section.

EXECUTIVE SUMMARY

In support of the joint effort among The University of California, Boeing, and SRI International to evaluate the use of Zylon fabric for engine rotor burst debris shields on commercial transport aircraft, Boeing designed a series of ballistic tests intended to evaluate the ballistic performance of Zylon fabric for airplane engine rotor burst shielding. The tests were executed by the University of California (small-scale laboratory tests) and SRI International (large-scale (airplane size) tests). This appendix contains the initial test plan for both of these tests. This part of the FAA report contains the results of the airplane scale tests.

Two series of tests were designed. One series focused on small-scale tests intended to provide a significant number data points for relatively simple test configurations conducted in a laboratory environment. In these tests 10 in. x 10 in. (254 mm x 254 mm) Zylon targets and 0.50 in. (12.7 mm) diameter cylindrical projectiles were used. Several different attachment conditions at the edges of the targets were considered. Projectile velocities in the range of 500-1000 ft/sec (153-305 m/sec) were specified.

The second set of tests focused on test articles on the scale of commercial airplane structure and rotor burst shields. Targets consisted of Zylon fabric and aluminum sheets of thickness similar to commercial airplane skins. The targets were mounted on relatively rigid steel frame structures with spacing between members similar to that of frames and stringers in modern commercial airplanes. Projectiles were designed to be representative of engine debris liberated by a rotor burst event. Two fragments were used. The smaller was a 2.0 in. x 2.0 in. x 0.25 in. (50.8 mm x 50.8 mm x 6.4 mm) rectangular parallelepiped made from steel and intended to be similar in size and mass to a high pressure turbine blade. The larger fragment was a 4.0 in. x 4.0 in. x 0.50 in. (101.6 mm x 101.6 mm x 12.7 mm) rectangular parallelepiped made from steel which was intended to be similar in size and mass to a partial fan blade fragment. The smaller projectiles were specified to have incident velocities in the range of 500-1000 ft/sec (153-305 m/sec), and the larger fragments were specified to have velocities in the range of 400-700 ft/sec (122 – 214 m/sec). These velocities are typical of engine rotor burst debris fragments. Results of the large-scale aircraft size ballistic tests are included in this part of the FAA report.

A1. INTRODUCTION AND BACKGROUND.

The overall purpose of this effort was to evaluate the use of Zylon fabric for engine rotor burst debris shields on commercial transport aircraft. The Boeing effort was to independently evaluate Zylon material properties and to determine the effect of typical aircraft environments on Zylon fibers and to design a series of tests to evaluate the ballistic performance of Zylon fabric for airplane engine rotor burst shielding. This appendix describes the series of ballistic experiments designed. The results of the Zylon material property evaluation conducted by Boeing appear in part of this FAA report.

A2. SMALL-SCALE LABORATORY TESTS OF ZYLON FABRIC BALLISTIC PERFORMANCE.

Two sets of tests were designed to experimentally evaluate the ballistic performance of Zylon fabric for transport airplane rotor burst shielding applications, one of which is described in this Section. Small-scale ballistic tests were designed to permit the ballistic properties of Zylon fabric targets to be evaluated from a relatively large number of experiments in a controlled laboratory setting. This series of experiments was designed to be conducted in the Gun Laboratory of the Department of Mechanical Engineering of the University of California at Berkeley, and the experiments were designed to make use of existing equipment in the laboratory. For this reason, 0.50 in. (12.7 mm) cylindrical projectiles used in this series of tests, as a smooth barrel 0.50 caliber powder gun was available. The projectiles were machined from steel and clad with copper to avoid damage to the gun barrel. Their mass was 0.083 lb (37.2 g). The projectiles were incident upon the targets with velocities of 500-1000 ft/sec (153-305 m/sec), which are typical of debris fragments liberated by transport airplane engine rotor burst events. Normal and oblique angles of incidence were specified.

Four series of targets were proposed. The first series consisted of square 10 in. x 10 in. (254 mm x 254 mm) bare fabric targets as indicated in Figure A1. The fabric targets were to be held in a frame-like fixture that would ensure that all four edges of the target remained nearly fixed during impact with the projectiles. Targets were to be installed without slack in the fabric. The projectiles were to impact the target at locations in the center of the targets and at locations closer to a corner, as indicated in Figure A1. Several thicknesses of Zylon fabric were to be tested as targets. It was intended that for each target thickness projectiles with a range of incident velocities would be used, so that performance of the target at projectile velocities above and below the ballistic limit for that target/projectile pair could be measured. In addition, targets of Kevlar fabric were to be tested as well to provide an indication of the relative ballistic performance of Zylon and Kevlar fabrics.

The second series of laboratory tests is shown schematically in Figure A2. This series of tests was designed to be similar to those of Figure A1 except for the way that the fabric targets were to be attached to the target holders. In this series of tests, the fabric target was to be attached to the target holder at discrete locations by bolts and washers. Cases of four attachment points at the corners of the target holder and eight attachment points at the corners and mid points of the sides of the target holder were specified, as indicated in Figure A2. The targets in this series of tests were to be bare Zylon fabric. Impact points at the center of the target and near one of its corners are specified, as indicated in Figure A2. The projectile and incident velocities specified are similar to those specified for the previous test series with clamped fabric edge conditions.

The third series of laboratory tests specified is shown in Figure A3. This series of tests is similar to those shown in Figure A1 except that the target consists of aluminum sheet in addition to Zylon fabric. The objective of this test series is to determine if the reinforcement of the aluminum sheet by the Zylon fabric would result in greater shielding performance than one would expect from the aluminum sheet and the Zylon fabric without any interaction. For this reason, the spacing between the aluminum sheet and the Zylon fabric is variable, as indicated in Figure A3. Like the test series of Figure A1, clamped edge conditions were to be imposed on the

fabric and aluminum sheet by the target holder. The projectile and incidence conditions specified were similar to those of the previous two small-scale test series.

The fourth series of small-scale ballistic tests was intended to determine the ballistic performance of Zylon fabric under simultaneous impacts by multiple projectiles. The test configuration is shown in Figure A4. Targets were specified to be 10 in. x 10 in. (254 mm x 254 mm) bare Zylon fabric held in target holders imposing clamped edge conditions similar to those used in the test series of Figure A1. Projectiles were specified to be spherical buckshot fired simultaneously from a shotgun arrangement. Projectile velocities in the range of 500-1000 ft/sec (153-305 m/sec) were specified. Incidence was specified to be normal to the target with the centroid of the projectile group nominally located at the target center.

For all cases of target configuration and projectile incidence conditions it was expected that experiments would be repeated one time or more to permit some measure of uncertainty in the experimental results. In this case test configurations of Figures A3 and A4 were not completed due to resource limitations, and an additional test series with clamped conditions on two sides similar to that of Figure A1 was conducted.

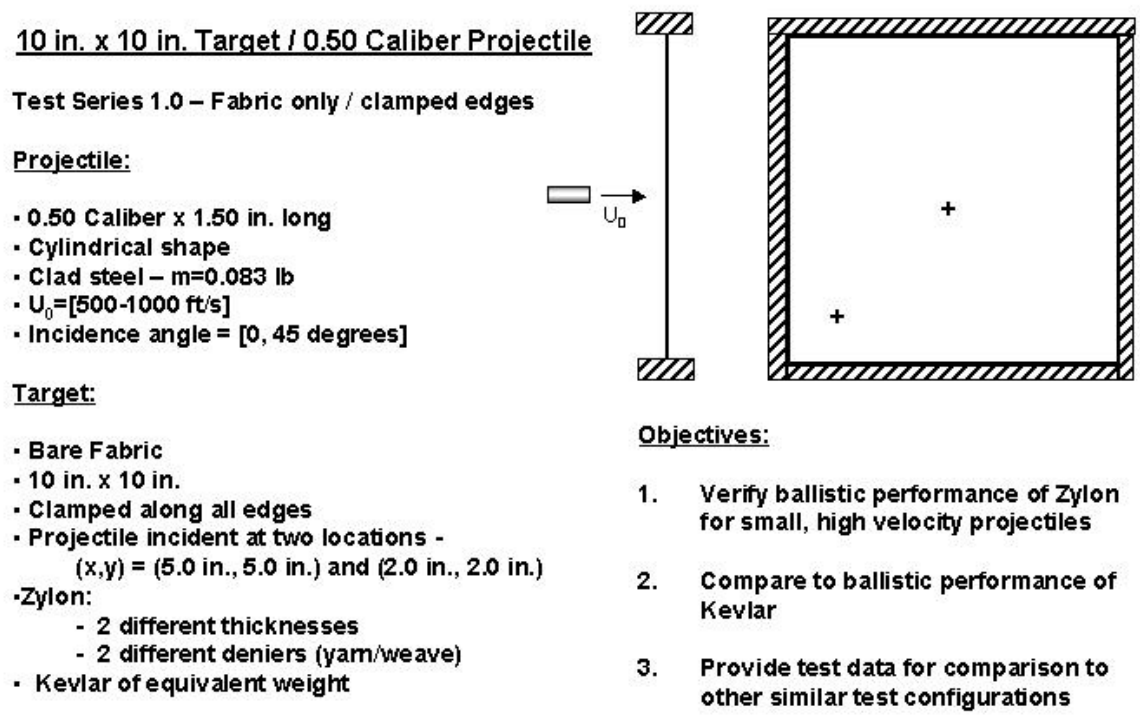

Figure A1. Schematic for small-scale laboratory test of Zylon fabric ballistic properties: bare fabric targets with clamped edge conditions

10 in. x 10 in. Target / 0.50 Caliber Projectile

Test Series 2.0 – Fabric only / bolted edges

Projectile:

- 0.50 Caliber x 1.50 in. long
- Cylindrical shape
- Clad steel – m=0.083 lb
- U_0=[500-1000 ft/s]
- Incidence angle = [0, 45 degrees]

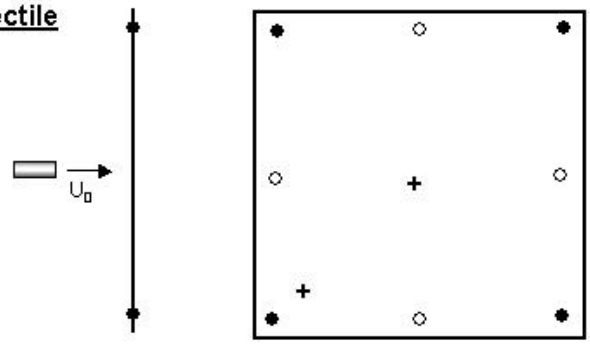

Target:

- Bare Fabric
- 10 in. x 10 in.
- Bolted at 4 – 8 discrete locations (with washers)
- Projectile incident at two locations -
  (x,y) = (5.0 in., 5.0 in.) and (2.0 in., 2.0 in.)
- Zylon:
  - 2 different thicknesses

Objectives:

1. Determine effect of fabric edge conditions on relative ballistic performance of Zylon shields

Figure A2. Schematic for small-scale laboratory test of Zylon fabric ballistic properties: bare fabric targets with edges constrained by discrete fasteners

10 in. x 10 in. Target / 0.50 Caliber Projectile

Test Series 3.0 – Aluminum + Zylon / clamped edges

Projectile:

- 0.50 Caliber x 1.50 in. long
- Cylindrical shape
- Clad steel – m=0.083 lb
- U_0=[500-1000 ft/s]
- Incidence angle = [0, 45 degrees]

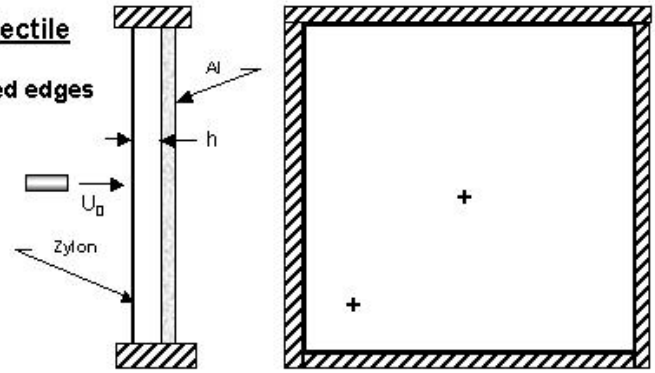

Target:

- Aluminum (2024-T4) sheet / Zylon fabric shield
- 10 in. x 10 in. - Clamped along all edges
- Cases of Zylon before Al and Zylon after Al to be considered
- Projectile incident at two locations - (x,y) = (5.0 in., 5.0 in.) and (2.0 in., 2.0 in.)
- Zylon - 2 different thicknesses
- Aluminum – 2 different thicknesses
- Spacing h – [0, 0.5 in.]

Objectives:

1. Determine effect of interaction of Zylon with adjacent metal structure on ballistic performance of Zylon fabric shields – small, high velocity projectiles
2. Investigate both shielding and containment configurations

Figure A3. Schematic for small-scale laboratory test of Zylon fabric ballistic properties: aluminum sheet and Zylon fabric targets with clamped edge conditions

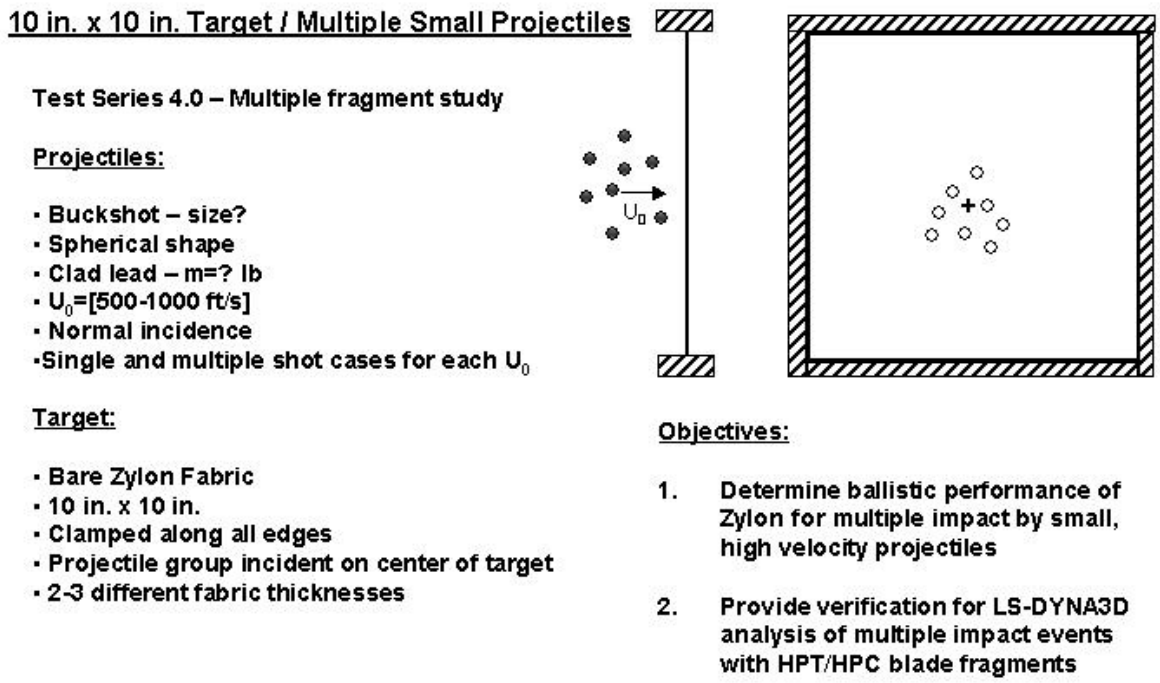

Figure A4. Schematic for small-scale laboratory test of Zylon fabric ballistic properties: Multiple simultaneous projectiles with clamped edge conditions

A3. AIRPLANE SCALE TESTS OF ZYLON FABRIC BALLISTIC PERFORMANCE.

The set of tests described in this Section was intended to resemble possible installations of Zylon fabric on transport airplanes for rotor burst debris shielding. These experiments were designed to be conducted by SRI International at their 6 in. (152.4 mm) gas gun range. Two projectiles were specified for use in these tests. The smaller was a 2.0 in. x 2.0 in. x 0.25 in. (50.8 mm x 50.8 mm x 6.4 mm) rectangular parallelepiped made from steel and intended to be similar in size and mass to a high pressure turbine blade. The larger fragment was a 4.0 in. x 4.0 in. x 0.50 in. (101.6 mm x 101.6 mm x 12.7 mm) rectangular parallelepiped made from steel which was intended to be similar in size and mass to a partial fan blade fragment. The smaller projectiles were specified to have incident velocities in the range of 500-1000 ft/sec (153-305 m/sec), and the larger fragments were specified to have velocities in the range of 400-700 ft/sec (122 – 214 m/sec). Only normal incidence conditions were specified for the airplane-scale tests.

The configuration specified for the first series of airplane-scale experiments is indicated in Figure A5. The targets for these tests consisted of Zylon fabric and aluminum sheet metal attached to a steel ladder frame by bolts and washers. The ladder frame arrangement was intended to have spacing between horizontal and vertical members similar to the spacing between frames and stringers in typical commercial airplane fuselage structures. The ladder frame was to be designed such that it would not yield under the loads imposed by impact with the projectiles so that it could be re-used in subsequent tests. The aluminum sheet was to be placed in front of the Zylon fabric, like the small-scale experiments of Figure A3. Unlike those experiments, test cases involving targets with Zylon fabric only were specified. Cases of projectile velocities resulting in penetration and nonpenetration were specified for both projectiles.

The configuration for another series of airplane-scale tests is shown in Figure 6. These tests were intended to be similar to a possible installation of Zylon fabric on the interior of an airplane engine fan cowl. The test configuration involved Zylon fabric and aluminum sheet attached to vertical steel frame sections by bolts and washers. In addition, bolts and washers between the fabric and aluminum sheet were specified at a grid of so-called “field” points between the support frames. Like the ladder frame test series, the steel support members were specified to be such that they would not experience plastic deformation during the tests. Again, cases of projectile velocities resulting in penetration and nonpenetration were specified for both projectiles. More than one impact location on the target was specified.

The final series of airplane-scale tests is shown in Figure A7. These tests involved Zylon fabric installed on a section of Boeing airplane fuselage structure. The tests were intended to permit evaluation of the ballistic performance of Zylon fabric interacting with insulation blankets, trim panels, and other airplane fuselage components. It was anticipated that sections salvaged from a Boeing 727 airplane would be used for this test, as they were available to SRI International. Impact by both projectiles for the airplane series tests were specified, with incidence conditions resulting in penetration and nonpenetration for each.

For all cases of target configuration and projectile incidence conditions, it was expected that experiments would be repeated one time or more to permit some measure of uncertainty in the experimental results.

The tests actually performed by SRI deviated somewhat from the plan originally proposed. The most significant change was the deletion of the test series of Figure A7 due to resource limitations.

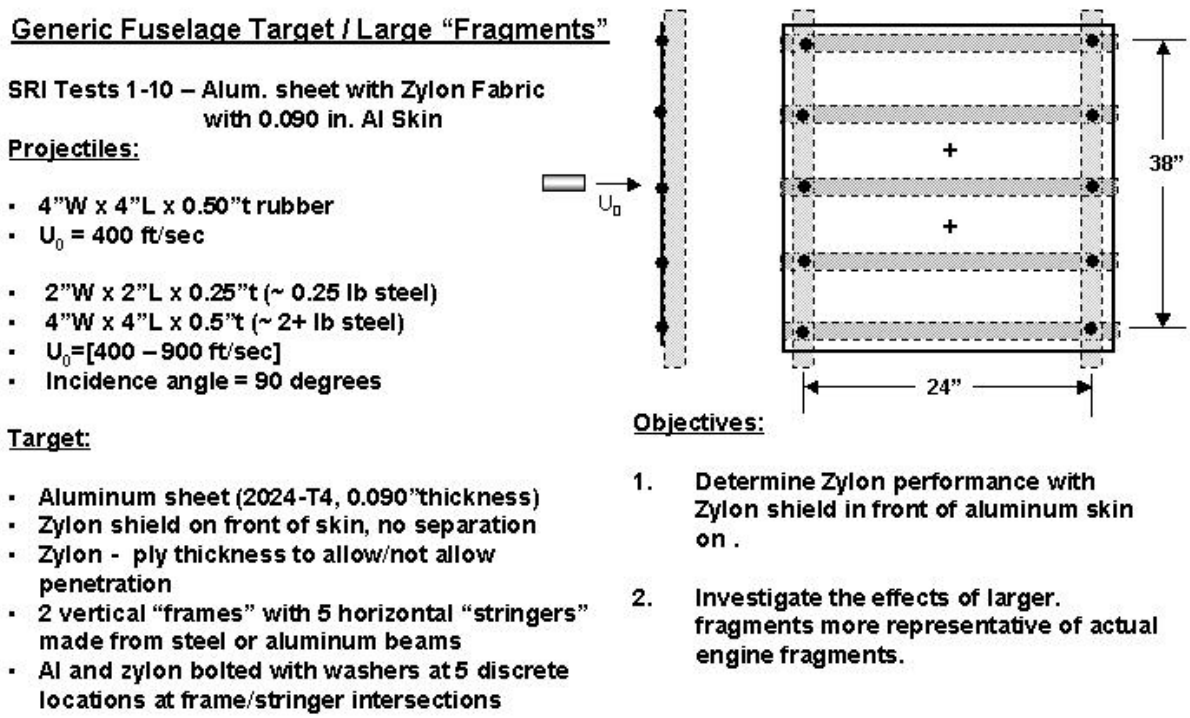

Figure A5. Schematic for airplane scale test of Zylon fabric ballistic properties: aluminum sheet and Zylon fabric targets attached to ladder frame similar to commercial airplane structure

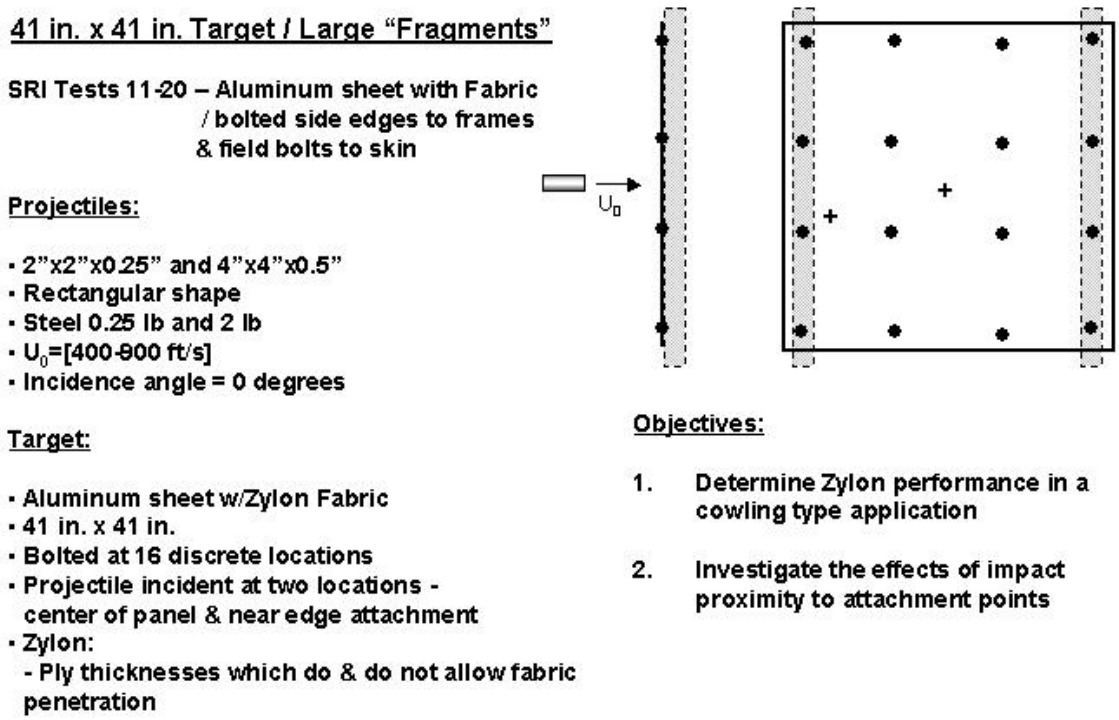

Figure A6. Schematic for airplane scale test of Zylon fabric ballistic properties: aluminum sheet and Zylon fabric targets attached to steel frame similar to commercial airplane fan cowl structure

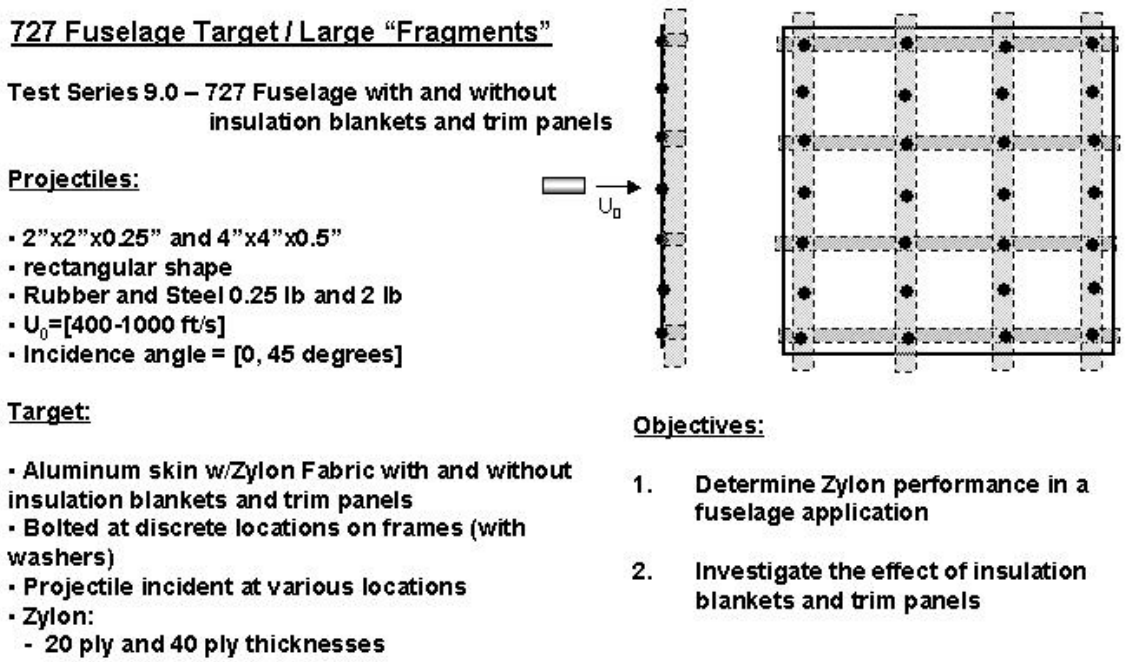

Figure A7. Schematic for airplane scale test of Zylon fabric ballistic properties: Zylon fabric shield installed of salvaged transport airplane fuselage section.

4. CONCLUSION.

Two series of tests have been designed to permit evaluation of the ballistic performance of Zylon fabric for use as engine rotor burst debris shield material in commercial airplanes. This report describes the sets of experiments as originally specified by Boeing. As The University of California and SRI International pursued their respective ballistic test programs, deviations from this test plan were chosen. In some cases tests series were eliminated due to lack of time and resources available to complete them, in other cases additional target configurations were added in attempts to improve the degree to which conditions of the targets and projectiles could be controlled.